

Project information

Project full title	Connecting Russian and European Measures for Large-scale Research Infrastructures – plus
Project acronym	CREMLINplus
Grant agreement no.	871072
Instrument	Research and Innovation Action (RIA)
Duration	01/02/2020 – 31/01/2024
Website	www.cremlinplus.eu

Deliverable information

Deliverable no.	D2.5 (D10)
Deliverable title	Simulation results for selected observables
Deliverable responsible	Mephi
Related Work-Package/Task	WP2.3
Type (e.g. Report; other)	Report
Author(s)	Arkadiy Taranenko
Dissemination level	Public
Document Version	final
Date	20.01.2022
Download page	

Document information

Version no.	Date	Author(s)	Comment
1	16.12.2021	Oleg Golosov Evgeny Kashirin Petr Parfenov Ilya Selyuzhenkov Peter Senger Arkadiy Taranenko	Simulation results for selected observables WP2.3



Table of Contents:

1. Introduction
2. Performance studies for the CBM experiment at FAIR
 - 2.1 Procedure for charged hadrons identification in the CBM experiment
 - 2.2 Application of the MC-Glauber model for centrality determination
 - 2.3 Performance for anisotropic flow measurement in the CBM experiment
 - 2.4 Summary
3. Performance studies for the MPD experiment at NICA
 - 3.1 Procedure for charged hadrons identification in the MPD experiment
 - 3.2 Methods for centrality determination based on charged particle multiplicity
 - 3.2.1 MC-Glauber method
 - 3.2.2 Inverse Bayesian method (Γ -fit method)
 - 3.2.3 Comparison of the methods
 - 3.3 Flow Performance for anisotropic flow measurements
 - 3.4 Summary
4. Summary and outlook
5. Publications 2020-2021



1. Introduction

The FAIR and NICA accelerator facilities will execute experiments to explore the properties of QCD matter at neutron star core densities. The research programs will be performed at FAIR with the Compressed Baryonic Matter (CBM) experiment, and at NICA with the Multi-Purpose Detector (MPD) setup at the collider, and with the Baryonic Matter at Nuclotron (BM@N) experiment at the Nuclotron. These three experiments are complementary, with respect to the beam energy [1]. The development of common software packages for simulation and data analysis for BM@N and MPD experiments at NICA and the CBM experiment at FAIR has been started. In this report, we discuss the anticipated performance of the developed common frameworks for centrality determination and anisotropic flow measurements of identified hadrons.

2. Performance studies for the CBM experiment at FAIR

Performance of the Compressed Baryonic Matter (CBM) experiment for the measurement of proton and positively charged kaon directed flow is presented as a function of collision centrality, particle transverse momentum and rapidity. The analysis is based on Au+Au collisions at the top SIS100 beam momentum of 12A GeV/c simulated with the DCM-QGSM-SMM [2] event generator and transported through the CBM material using GEANT4 [3] Monte-Carlo package. The calculations of flow coefficients are performed with respect to the projectile spectator symmetry plane. Data-driven procedures for centrality determination, particle identification and symmetry plane reconstruction are developed and used in the performance studies. Dependence of the results on the details of the spectator symmetry plane estimation and purity of particle identification are studied by comparing the reconstructed signals with the event generator input.

The tracking system of the CBM experiment consists of Micro-Vertex Detector (MVD) and Silicon Tracking System (STS) which are located inside the magnetic field. The polar angle acceptance of the tracking system is $2.5^\circ < \theta < 25^\circ$. The MVD and STS can be used to calculate multiplicity of the produced charged pions using reconstruction procedure of the charged particles tracks.

2.1 Procedure for charged hadrons identification in the CBM experiment

Identification of charged hadrons in CBM will be performed using time of flight information from the TOF detector [4]. TOF will be located at 7 meters downstream the target with acceptance in polar angle between 2.5° and 25° . Its layout is presented in Fig. 1.



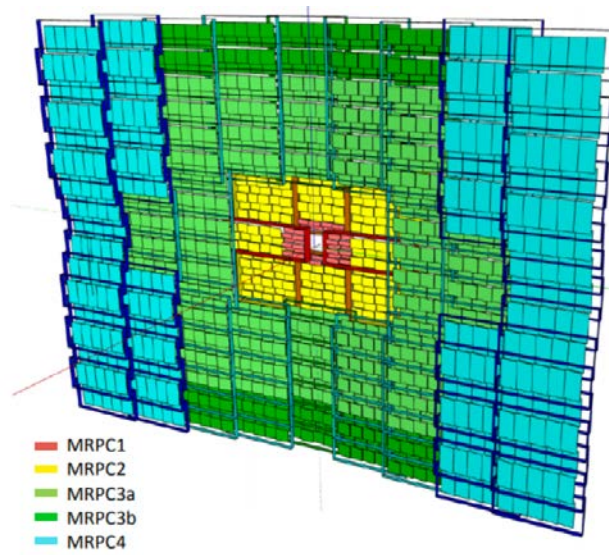


Figure 1: CBM Time of flight detector layout.

Particle identification via time-of-flight is based on simultaneous measurement of momentum p , time t and track length l of a particle using the relation to its squared mass m^2 :

$$\frac{m^2}{q^2} = p^2 \left(\frac{t^2 c^2}{l^2} - 1 \right) \quad (1)$$

where: p - momentum obtained from tracking system; q - particle charge; c - speed of light; t - time of flight from the TOF system relative to event start; l - length of trajectory from collision primary vertex to the TOF hit location.

To develop an automated procedure for Particle Identification (PID) a sample of 5M Au+Au collisions with beam momentum of 12A GeV/c produced with DCM-QGSM-SMM event generator were used. Simulation of CBM detector response was performed using GEANT4 transport engine. Simulation was performed for the full detector setup including beam pipe, magnet, MVD, STS, RICH, TRD, PSD and TOF. Realistic procedures implemented in the CBMROOT framework were used for event reconstruction. For this analysis we used reconstructed tracks with at least 4 hits in STS and MVD, fit quality $\chi^2/\text{NDF} < 3$ and distance to primary vertex normalized to its error $\chi^2_{\text{prim}} < 3$. Distribution of particle squared mass versus momentum for different particle species is presented in figure 2.



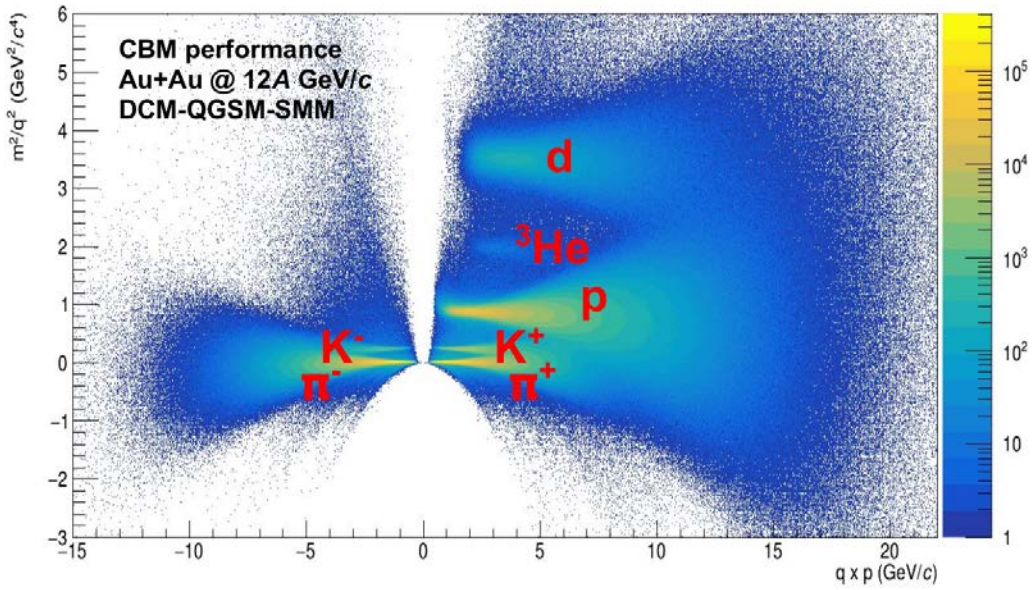


Figure 2. Distribution of particle squared mass versus momentum.

PID procedure is similar to that developed in ALICE [5]:

1. Fill m^2 vs p distributions for pure samples of π , K and p (denoted below as 2D-(π ,K,p)) and for all particles (2D-all). Pure samples of pions, kaons and protons can be obtained from decay daughters of K^0_s , Λ and ϕ mesons using the KF Particle Finder [6].
2. Parameterize m^2 distribution in slices of momentum:
 - a. Fit each slice of 2D-(π ,K,p) using Gaussian function $G(m^2) = A \times \exp(-0.5(|m^2 - \mu|/\sigma)^2)$ with 3 parameters: abundance (A), mean (μ), sigma (σ).
 - b. Fit each slice of 2D-all with a sum of Gaussians $G(m^2, p)$ and polynomial function for background $BG(m^2, p)$.
 - c. Parametrize momentum dependence of the fit parameters. Repeat until parameters are stabilized.
 - d. Save fit parameters to the ROOT file for further use in the analysis.
3. Calculate a bayesian probability P_j for a given m^2 and p for a particle to be of type j :

$$P_j(m^2, p) = \frac{G_j(m^2, p)}{\sum_{i=\pi, p, K} G_i(m^2, p) + BG(m^2, p)} \quad (2)$$

This procedure should be applied in different centrality classes. Figure 1 is an illustration of the PID procedure using Gaussian fit function ($k = 2$ and $s = 0$ in $G(m^2)$). A pure sample of particles is obtained using Monte Carlo true information. Figure 2 shows distributions of momentum versus squared mass for the tracks identified as protons, positive kaons and positive pions with 90% purity.



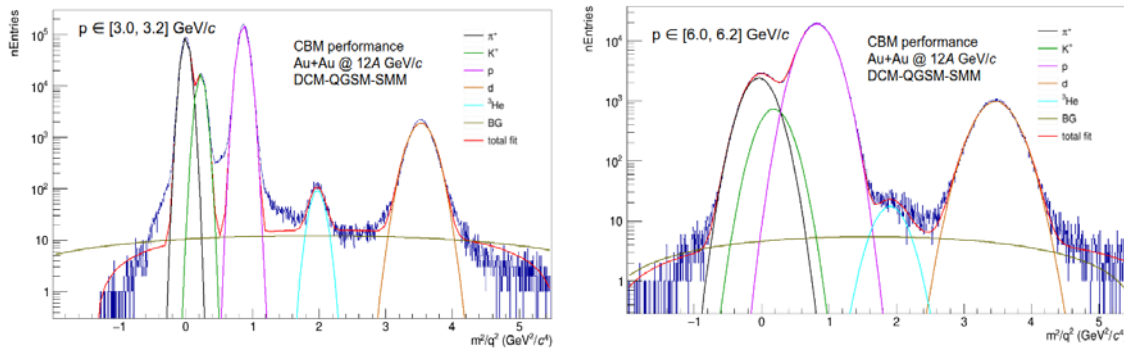


Figure 1. Illustration of the PID determination procedure using Gaussian fit function in two momentum slices: 3-3.2 GeV/c (left) and 6-6.2 GeV/c (right)

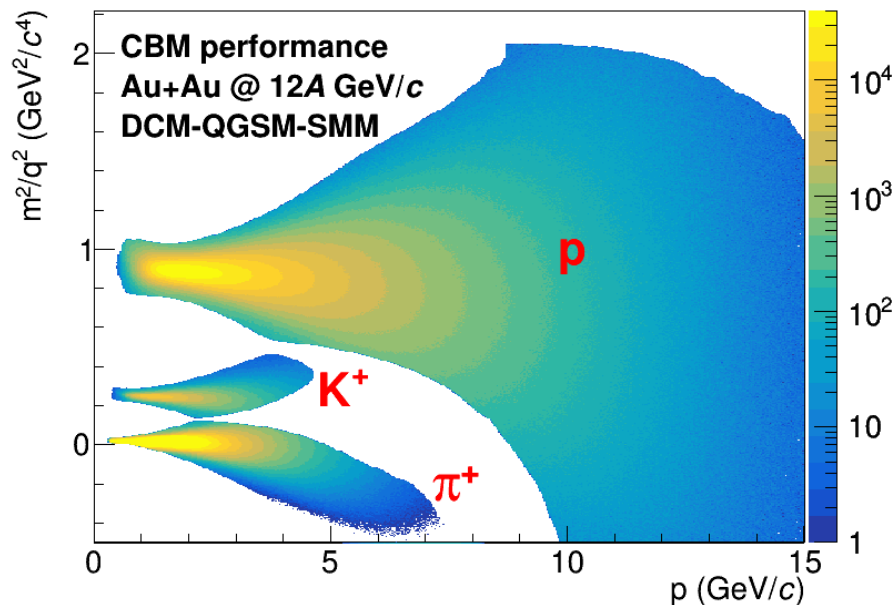


Figure 2. Distributions of momentum versus squared mass for the tracks identified as protons, positive kaons and positive pions with 90% purity.

2.2 Application of the MC-Glauber model for centrality determination

Centrality is an important concept in the study of strongly interacting matter created in a heavy-ion collision whose evolution depends on its initial geometry. Experimentally collisions can be characterized with the measured multiplicities or energy of produced particles at midrapidity or spectator fragments emitted in the forward rapidity region. Relation between collision geometry and experimentally measured multiplicities is commonly evaluated within the Monte-Carlo Glauber approach [7]. Centrality determination for the CBM based on multiplicity of produced particles and Monte-Carlo Glauber has been developed.



This project has received funding from the European Union's Horizon 2020 research and innovation programme under grant agreement No. 871072.

Theoretically, initial geometry can be characterized by impact parameter (b), number of participants (N_{part}) and number of binary nucleon-nucleon collisions (N_{coll}). In terms of impact parameter (b) distribution the collision centrality, C_b :

$$C_b = \frac{1}{\sigma_{inel}^{AA}} \int_0^b \frac{d\sigma}{db'} db' \quad (3)$$

Here b is the impact parameter and $d\sigma/db$ is the differential cross-section of a nuclei collision. Events with centrality 0% correspond to the most central collisions with low number of spectators and small impact parameter values ($b \approx 0$ fm).

Experimentally, collision geometry can be characterized, for example, by the measured multiplicity of produced charged particles. All events are sorted into groups called centrality classes according to their multiplicity. The most central (or peripheral) events with the highest (or lowest) multiplicity correspond to the value of centrality close to 0% (or 100%). The corresponding group of central (or peripheral) collisions corresponds to the range of impact parameter values close to zero (diameter of the colliding nuclei). Relation between collision geometry and experimentally measured multiplicities is commonly provided with the Monte-Carlo Glauber approach. To avoid contamination of the collision spectators (e.g. protons) in centrality determination procedure only charged pions are used for multiplicity calculation. Figure 3 shows the multiplicity distribution of produced pions from the UrQMD event generator [8] compared to the reconstructed pion multiplicity using the GEANT4 Monte-Carlo simulation of the CBM experiment [9].

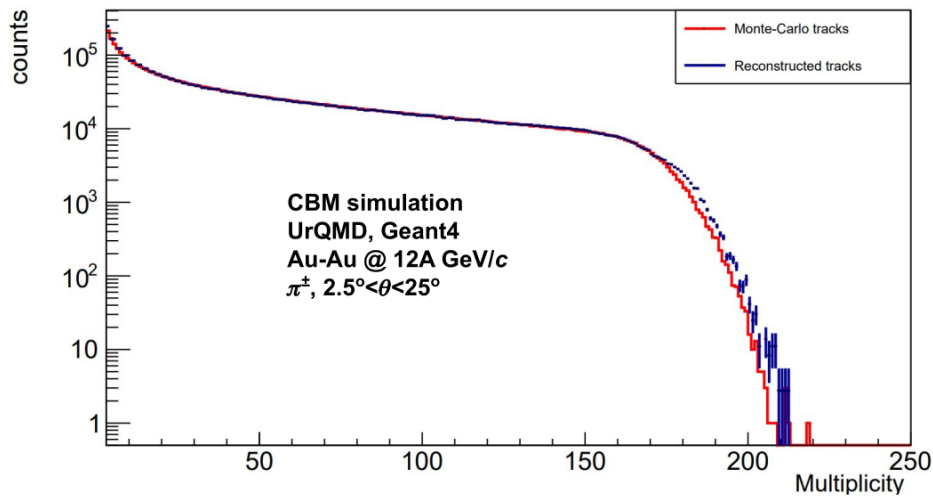


Figure 3: Comparison between the shape of the multiplicity distribution for true Monte-Carlo particles and reconstructed charged pions. Multiplicity of the reconstructed pions is scaled by 1.6.

Centrality percentiles with the produced charged pion multiplicity is calculated as:

$$C_M = \frac{1}{\sigma_{inel}^{AA}} \int_M^{\infty} \frac{d\sigma}{dM'} dM' \quad (4)$$



where M is a number of produced charged pions. Relation between impact parameter magnitude and multiplicity of charged pions is presented in Fig. 4.

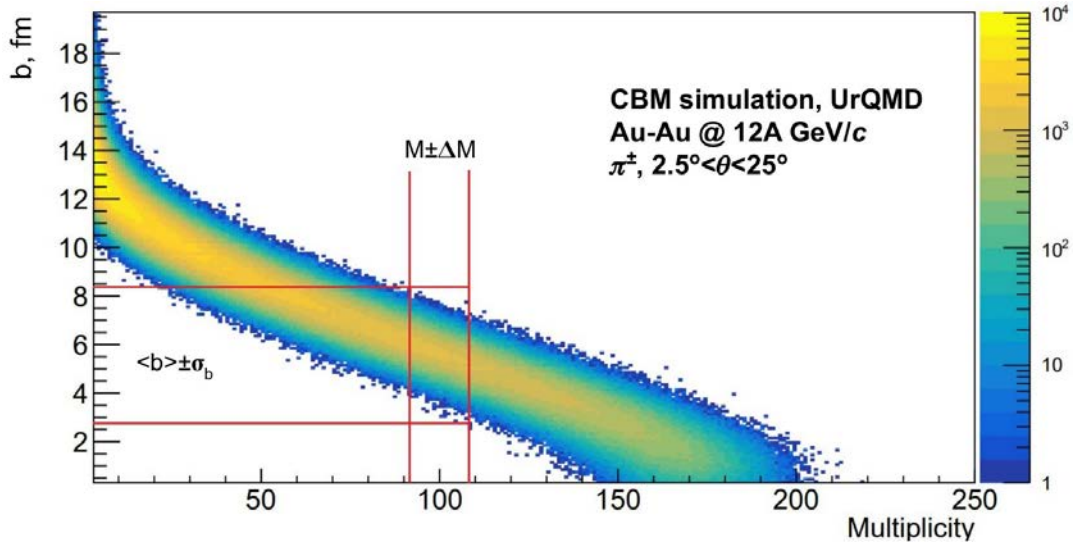


Figure 4: Distribution of the impact parameter magnitude and multiplicity of produced charged pions. Red lines illustrate the regions of the centrality class determined by multiplicity and the corresponding range of impact parameters.

Due to the spread of the multiplicity distribution at a given impact parameter value there is a smearing between centrality defined by Eq. (4) and the values of C_b given by Eq. (3). A Monte Carlo (MC) Glauber model is used for mapping multiplicity to the collision geometry. The MC-Glauber model is based on the following assumptions:

- Nucleus-nucleus collision is considered as a sequence of binary nucleon-nucleon collisions determined by the cross section of inelastic nucleon-nucleon interaction;
- The initial position of individual nucleons is sampled using Monte-Carlo simulation according to the Woods-Saxon distribution for the density of nuclear matter:

$$\rho(r) = \frac{\rho_0}{1 + \exp\left(\frac{r-R}{a}\right)} \quad (5)$$

where ρ_0 is the normalization coefficient, r is the distance to the center of the nucleus, R is the radius of the nucleus, and the parameter a is the depth of the skin layer;

- Individual nucleons move along straight trajectories during collision.

Multiplicity distribution of produced charged particles is fitted using the MC-Glauber model. For a given event with a number of participants N_{part} and number of nucleon-nucleon collisions N_{coll} the number N_o of ancestors (sources) is calculated using a two-component model. This model assumes



that nucleon-nucleon interactions have hard and soft contributions and that the average multiplicity of produced particles is proportional to a combination of N_{part} and N_{coll} :

$$N_a = fN_{part} + (1 - f)N_{coll} \quad (6)$$

where $f \in [0; 1]$ is a fit parameter. The number of produced particles per one ancestor is parametrized with a Negative Binomial Distribution (NBD):

$$P_{\mu,k}(n) = \frac{\Gamma(n+k)}{\Gamma(n+1)\Gamma(k)} \frac{(\mu/k)^n}{(\mu/k+1)^{n+k}} \quad (7)$$

where μ is an average multiplicity and k is responsible for the distribution width. The μ and k are also fit parameters. For each collision generated with the MC-Glauber model, the NBD is sampled N_a times in order to calculate the number of particles produced in this event. Multiplicity distribution is simulated for different values of NBD parameters μ , k and parameter f of the N_a . Then the minimization procedure is performed in order to evaluate parameters values μ , k , f which correspond to minimal χ^2 .

One million of Au+Au collisions at the beam momentum of 12A GeV/c were simulated with the UrQMD model. To reproduce acceptance of the CBM tracking system only charged pions generated with the $2.5^\circ < \theta < 25^\circ$ in the laboratory frame were accepted for analysis. Parameters of Woods-Saxon distribution were $R = 6.38$ fm and $a = 0.535$ fm. The cross section of inelastic nucleon-nucleon interaction was set to 30 mb. The best values of k and f parameters for minimal χ^2 were found by generating 10^7 MC-Glauber events and sampling model multiplicity distribution for each point of the parameter phase space is shown in Fig. 5. The grid of the parameter phase space was: $k \in [1, 30]$ with a step of 1, $f \in [0, 1]$ with a step of 0.02. Fit range included only regions with pion multiplicity above 50.



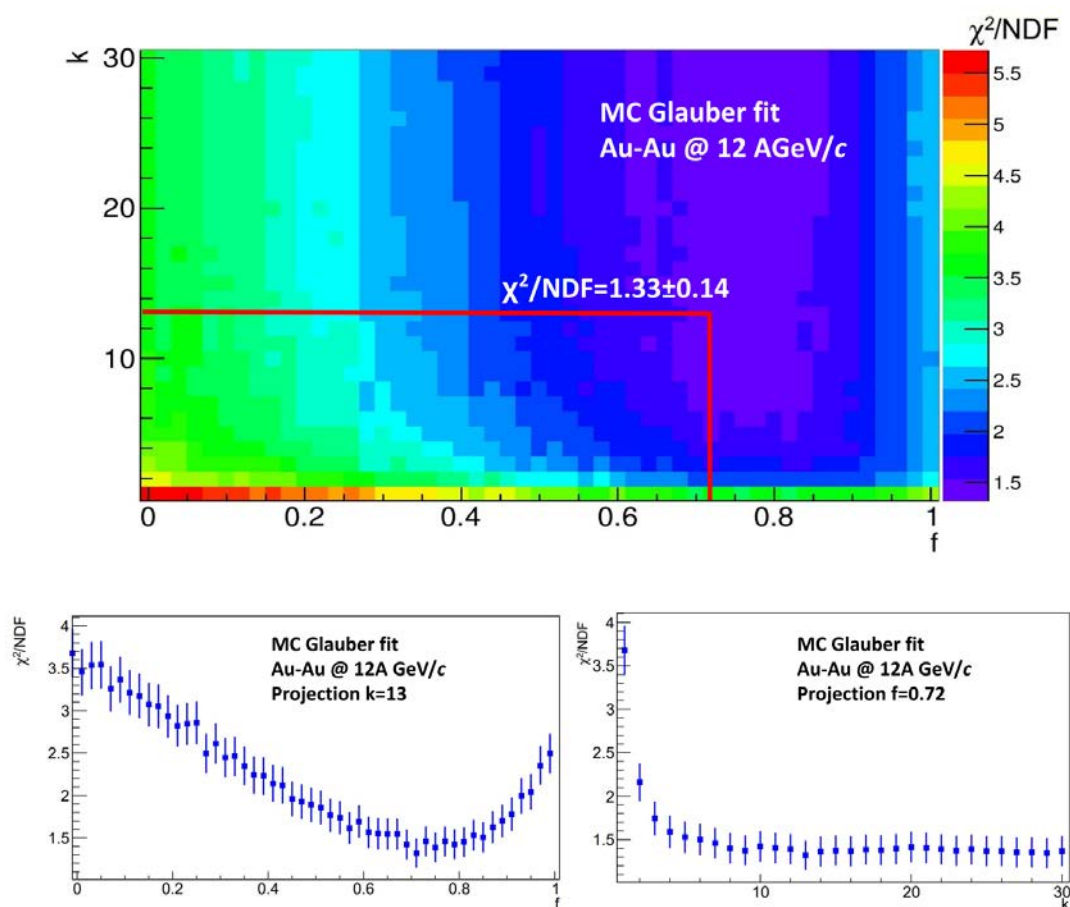


Figure 5: Upper panels: Illustration of the χ^2/NDF minimum search for the best values of the f and k parameters. Lower panels: Projections at the χ^2/NDF minimum: (left) at $k = 13$ and (right) at $f = 0.72$.

Results for the best fit are shown in Fig. 6. The left panel shows the result of the self-consistency check where distribution with known free parameters was fitted by the developed procedure. The right panel the result of fit of pion multiplicity distribution is shown. This fit reproduces multiplicity distribution in the whole fit range with minimal $\chi^2/\text{NDF} = 1.33 \pm 0.14$. The best fit parameters are $f = 0.72$, $k = 13$ and $\mu = 0.35$.

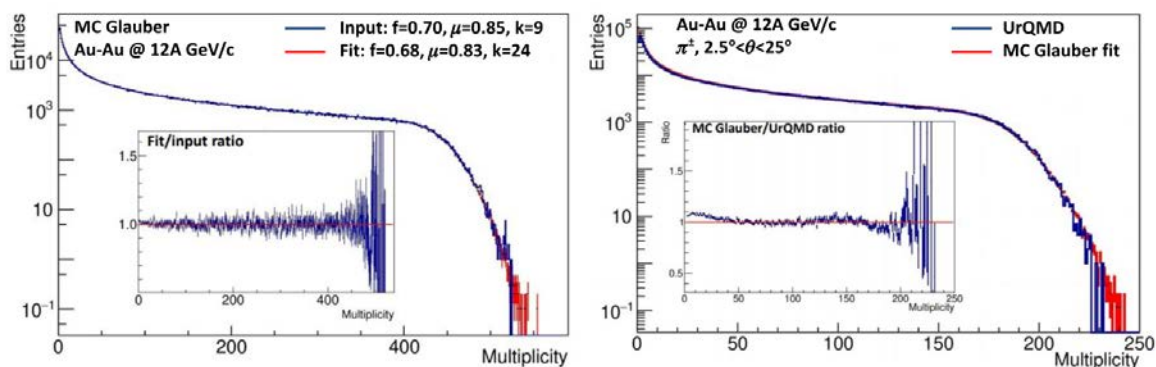


Figure 6: Results of the MC Glauber fits to the multiplicity distribution. Left: self-consistency check. Right: MC-Glauber fit to the multiplicity distribution of produced charged pions with UrQMD.

The result of the centrality determination procedure is presented in Fig. 7 (left), where the distributions of geometric parameters in various centrality classes are shown.

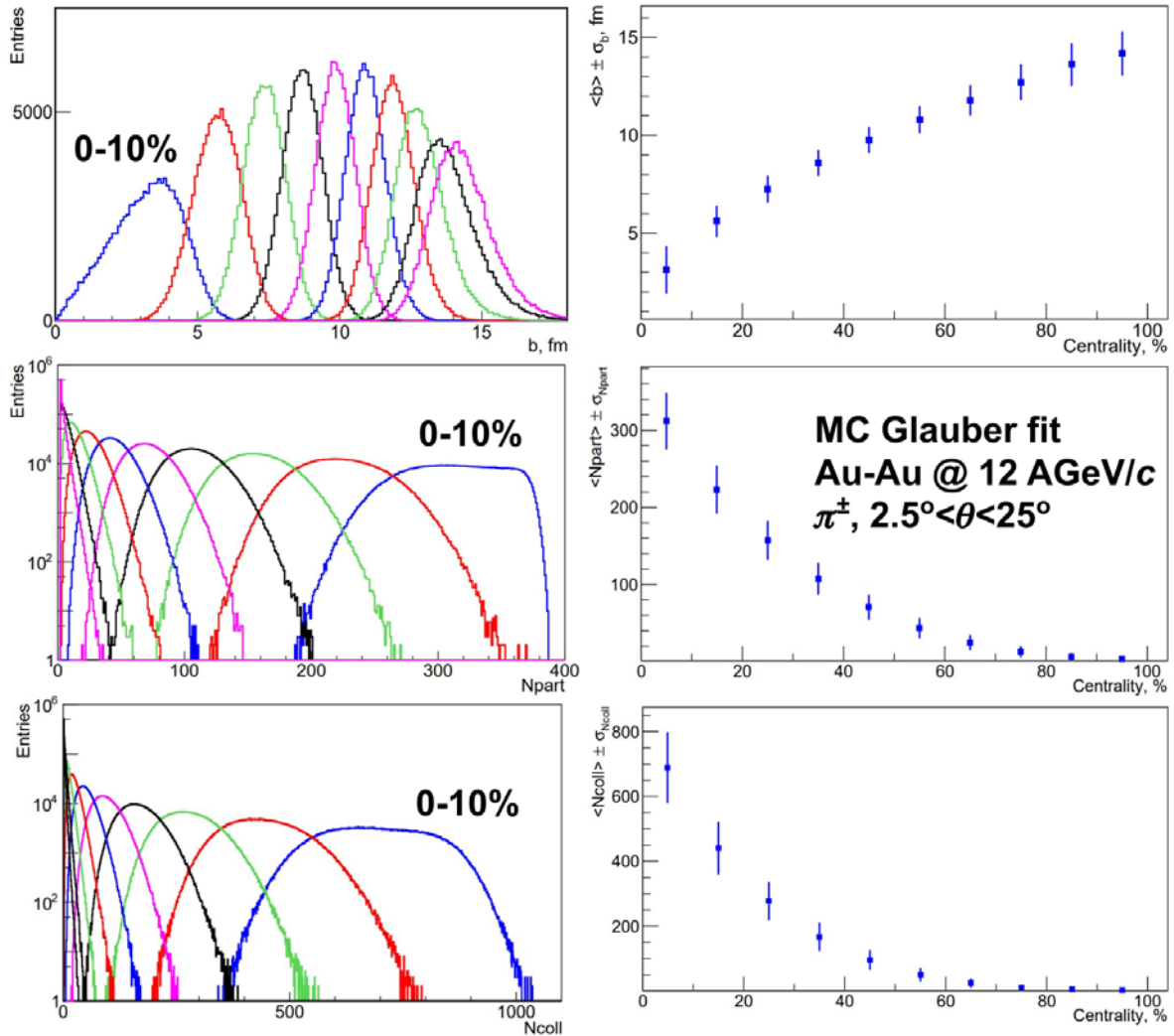


Figure 7: Distributions (left) and their corresponding average and a width (right) for the impact parameter (upper), N_{part} (middle) and N_{coll} (lower) in different centrality classes.

2.3 Performance for anisotropic flow measurement in the CBM experiment

Anisotropic transverse flow is one of the most important observables to probe the equation of state and transport properties of matter created in heavy-ion collisions. It is quantified with the anisotropic flow coefficients v_n [10] in a Fourier decomposition of azimuthal probability density ρ of produced particles relative to the collision symmetry plane given by the angle ψ_s :



$$\rho(\varphi - \Psi_s) = \frac{1}{2\pi} \left(1 + 2 \sum_{n=1}^{\infty} v_n \cos [n(\varphi - \Psi_s)] \right), \quad (8)$$

The most common example of the collision symmetry plane is the reaction plane defined by the impact parameter and beam direction. Due to the fluctuating position of the nucleons inside the colliding nuclei, different collision symmetry planes can be identified that are connected to the orientation of the matter in the nuclei overlap area and deflection of the spectator fragments in the plane transverse to the moving ions (Ψ_{SP}). v_n can be calculated using the following formula

$$v_n = \left\langle \cos n(\varphi - \Psi_s) \right\rangle, \quad (9)$$

where the angle brackets indicate averaging over all particles in all events. In the case of fixed-target experiments, usually, only projectile spectators can be measured. In the CBM experiment, the projectile spectator plane can be estimated using the transverse energy distribution in the Projectile Spectator Detector (PSD), from which a corresponding angle Ψ_{PSD} can be calculated. Taking into account the finite resolution of the Ψ_{PSD} angle with respect to the projectile spectator plane angle Ψ_{SP}^p , equation (9) is modified as:

$$v_n = \frac{\left\langle \cos n(\varphi - \Psi_{PSD}) \right\rangle}{R_{PSD}}, \quad (10)$$

where R_{PSD} is the PSD event plane resolution:

$$R_{PSD} = \left\langle \cos (\Psi_{SP}^p - \Psi_{PSD}) \right\rangle. \quad (11)$$

The magnitude of this correction factor may vary with the detector acceptance, collision energy, collision centrality, etc. To calculate the resolution correction factor R_{PSD} in real-data analysis, different data-driven methods are used. All of them are based on the analysis of correlations between azimuthal angles of different non-overlapping subsets of produced particles or spectator fragments, which are called subevents.

In this report, we present methods for the resolution correction factor extraction and the CBM performance for the projectile spectator symmetry plane estimation as a function of centrality for collisions of gold ions with a beam momentum of 12A GeV/c generated with the hybrid model combining the Dubna Cascade, Quark-Gluon String and the Statistical Multifragmentation Models (DCM-QGSM-SMM).

A sample of 5M collisions of gold ions with a beam momentum of 12A GeV/c generated with the DCM-QGSM-SMM model was used for this performance study. The DCM-QGSM-SMM generator is



characteristic for realistic modeling of spectator fragments which is crucial for the simulation of the PSD signals close to the one expected in the real experiment. The particles generated with the DCM-QGSM-SMM were passed through the GEANT4 simulation of the CBM detector response, and CBMROOT event and track reconstruction chain.

It is convenient to represent different estimates of the collision symmetry plane orientations in terms of two-dimensional flow (\mathbf{Q}_n) vectors defined in the plane transverse to the beam direction:

$$\mathbf{Q}_n = \frac{\sum_{i=1}^N w_i \mathbf{u}_{n,i}}{\sum_{i=1}^N w_i} \quad (12)$$

where

$$\mathbf{u}_{n,i} = (\cos n\phi_i, \sin n\phi_i). \quad (13)$$

\mathbf{Q}_n -vectors are calculated for the group of tracks reconstructed with MVD+STS or the groups of PSD modules with azimuthal angles ϕ_i . In equation (12), N is the total number of tracks (modules) in a subevent, i is the index of the track (module), and w_i is its weight equal to unity for tracks and to the energy deposition for PSD modules.

The rectangular shape of the detector subsystems and horizontal bending of charged particles' trajectories by the field of the CBM magnet introduce substantial biases in the azimuthal distributions used for the symmetry plane estimation. These biases were corrected for using the data-driven procedure described in [11] and implemented in the QnTools framework. A recentering correction was applied for all \mathbf{Q}_n -vectors. Additionally, twist and rescaling corrections were used for the \mathbf{Q}_n -vectors determined from the MVD+STS tracks. All corrections were applied as a function of the collision centrality.

Three different methods to calculate the first harmonic PSD resolution correction factor have been assessed in the study. 3-subevent method is given by equation:

$$R_{1,i}^A\{B,C\} = \sqrt{2 \frac{\langle Q_{1,i}^A Q_{1,i}^B \rangle \langle Q_{1,i}^A Q_{1,i}^C \rangle}{\langle Q_{1,i}^B Q_{1,i}^C \rangle}}, \quad (14)$$

where A , B and C mark different PSD subevents, while index i indicates the x and y components of the \mathbf{Q}_n -vector.

The mixed-harmonic method is an extension of the 3-subevent method with an additional projection on the 2-nd harmonic \mathbf{Q}_2^D -vector calculated from the MVD+STS subevents:



$$R_{1,i}^A\{B,C;D\} = \sqrt{2 \frac{\langle Q_{1,i}^A Q_{1,i}^B \rangle \langle Q_{1,i}^A Q_{1,j}^C Q_{2,k}^D \rangle}{\langle Q_{1,i}^B Q_{1,j}^C Q_{2,k}^D \rangle}}. \quad (15)$$

Non-zero correlations are possible for the following combinations: $(i, j, k) = (x, x, x), (x, x, y), (y, x, y)$ and (y, y, x) .

In the 4-subevent method, a fourth subevent is added that allows having a separation in rapidity between all correlated subevent pairs:

$$R_{1,i}^A = \sqrt{\frac{\langle Q_{1,i}^A Q_{1,i}^C \rangle R_{1,i}^D\{A,C\}}{\langle Q_{1,i}^C Q_{1,i}^D \rangle}}, \quad R_{1,i}^B = \frac{\langle Q_{1,i}^B Q_{1,i}^D \rangle}{R_{1,i}^D\{A,C\}}, \quad (16)$$

where a combination of (A, B, C, D) subevents can be either (PSD1, PSD2, PSD3, STS) or (PSD3, PSD2, PSD1, STS).

For each of the three methods, the results for x and y components of Q-vectors were compared with the resolution correction factors obtained using the reaction plane angle from the output of the DCM-QGSM-SMM event generator. These are given by equations analogous to equation (11) decomposed in a sum of cosine and sine products:

$$R_{1,x}^A = \langle \cos \Psi_{RP} Q_{1,x}^A \rangle, \quad R_{1,y}^A = \langle \sin \Psi_{RP} Q_{1,y}^A \rangle. \quad (17)$$

The different methods listed above were implemented using the following set of five subevents. Three subevents were defined from signals in groups of the PSD modules (Figure 1b): PSD1 (central modules), PSD2 (middle ring) and PSD3 (outer ring). Two additional subevents were defined from MVD + STS tracks identified as protons or positively charged pions using TOF information and the Bayesian approach:

- protons with $y \in [-0.6, -0.2]$ and $p_T \in [0, 3] \text{ GeV}/c$,
- positively charged pions with $y \in [0.8, 1.2]$ and $p_T \in [0, 1.4] \text{ GeV}/c$.

The negatively charged pions, which together with positive pions and protons constitute most of the produced hadrons, were excluded from consideration to avoid non-flow correlations with protons in the PSD acceptance due to secondary decays. The kinematic regions (see Figure 2) were chosen such that MVD + STS subevents contain particles with the larger magnitude of v_1 (to provide stronger subevent correlations) but are not in the acceptance of the PSD (to avoid self-correlations).

Figure 3a shows the resolution correction factors from the 3-subevent method for the three PSD subevents calculated using y components of \mathbf{Q}_1 -vectors. There are significant differences between the true (dashed lines) and reconstructed (colored symbols) resolution correction factors, in particular, for the PSD2 subevent that can be explained by the auto-correlations arising due sharing the hadronic



shower between modules in the neighboring subevents. For the PSD2 subevent, the affected correlations in equation (15) are $\langle Q_1^{\text{PSD1}} Q_1^{\text{PSD2}} \rangle$ and $\langle Q_1^{\text{PSD2}} Q_1^{\text{PSD3}} \rangle$.

To suppress effects due to correlations between neighbouring subevents, we deployed the mixed-harmonic method, which included an additional Q_2 -vector from the positively charged MVD + STS tracks identified using TOF information as pions. The results are shown in Figure 3b. The mixed-harmonic method allows reproducing true resolution correction factors for PSD1 and PSD3 using both x and y components of Q_1 -vectors. The method still does not fully remove the correlation between neighboring subevents in the case of the calculations for the PSD2 resolution correction. It should be noted that due to the smaller magnitude of the elliptic flow v_2 , the mixed-harmonic method requires much higher statistics compared to the 3-subevent method to obtain statistically stable results.

The 4-subevent method makes use of the auxiliary Q_1 -vector from STS and includes correlations only between rapidity-separated subevents. As can be seen from Figure 10a, the calculated resolution correction factors are in good agreement with the true values when the auxiliary subevent is constructed from positively charged MVD + STS tracks identified with TOF as pions. Using protons at backward-rapidity to construct the auxiliary subevent from MVD + STS tracks yields significantly worse performance and less stable results (see Fig. 10b), which indicates the presence of the remaining non-flow (resonances and other short range) correlations between protons in the MVD + STS acceptance and fragments registered by the PSD.



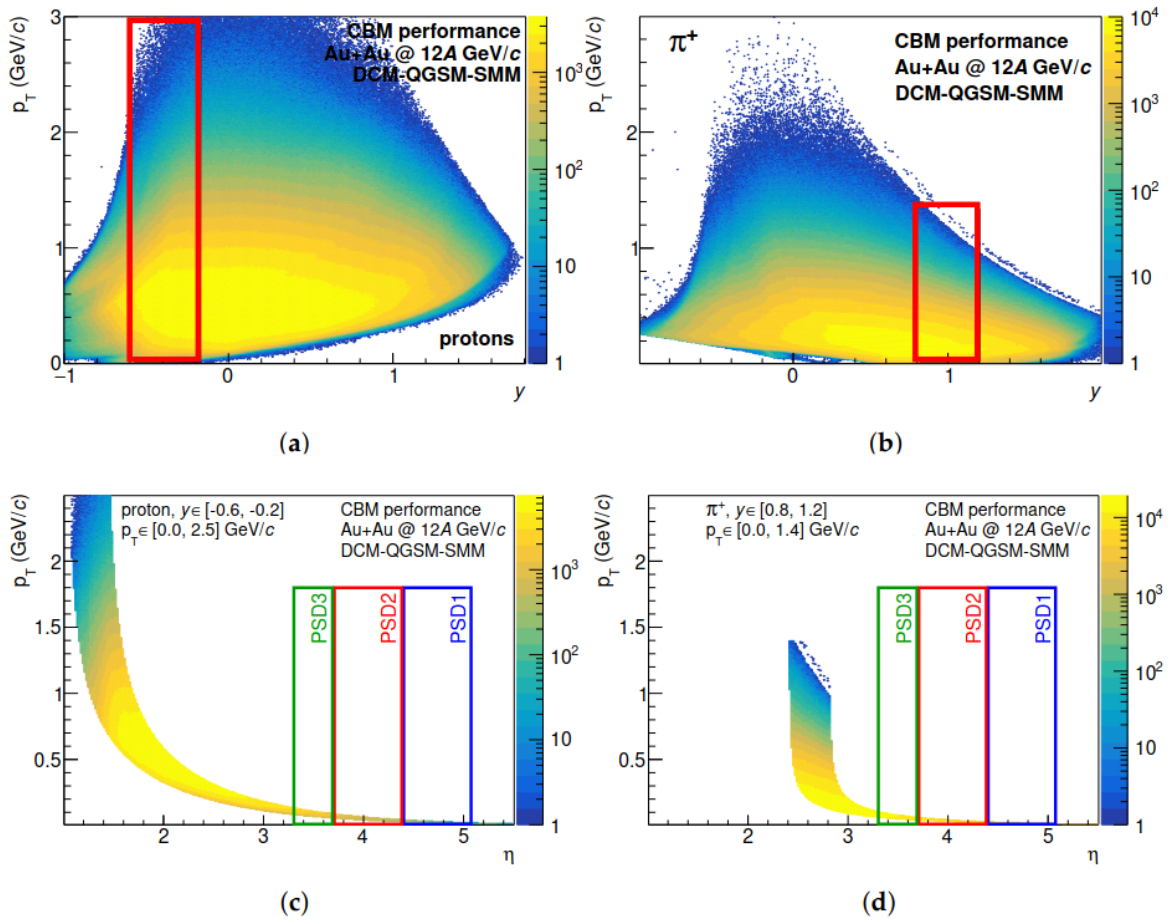


Figure 8. The distribution of tracks identified as (a) protons and (b) positively charged pions vs. p_T and y . Red boxes mark the kinematic selection for the corresponding Q-vector subevents. (c) and (d): comparison of the acceptance for the five (two STS and three PSD) subevents used in the performance studies. See text for details.

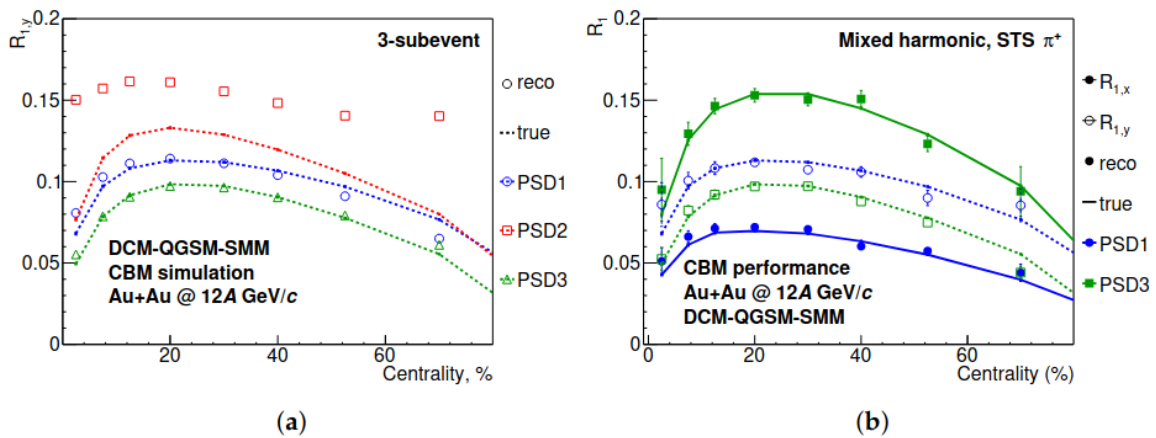


Figure 9. Resolution correction factors for PSD subevents calculated with (a) 3-subevent and (b) mixed-harmonic methods. The lines show the true values obtained using reaction plane angle from the event generator.

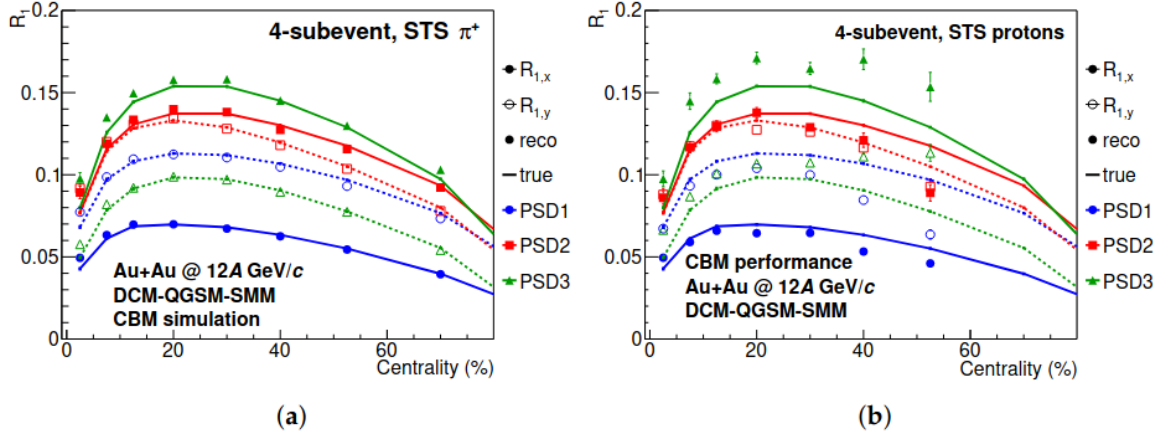


Figure 10. Resolution correction factors for PSD subevents calculated with the 4-subevent method using the auxiliary STS subevent from (a) positively charged pions and (b) protons. The lines show the true values of the resolution obtained using reaction plane angle from the event generator.

The scalar product method for directed flow v_1 was implemented using four Q-vector subevents. v_1 calculation is based on independent estimates from x and y components of the flow vectors and different PSD sub-events:

$$v_{1,i}\{A\} = \frac{2\langle q_i Q_{1,i}^A \rangle}{R_{1,i}^A\{B, C, D\}}. \quad (18)$$

Here $i = x, y$ denote \mathbf{q}_1 and \mathbf{Q}_1 components, $A, B,$ and C are different PSD subevents, and D is the \mathbf{Q}_1 -vector constructed using azimuthal distributions of the tracks identified as positively charged pions with $y \in [0, 1.2]$ and $p \in [0, 2]$. Finite resolution of symmetry plane estimation is corrected for by the resolution correction factors using the 4-subevent method.

Figure 11 shows the (p_T, y) population of the reconstructed tracks identified as protons, positively charged pions and kaons normalized to the (p_T, y) distributions obtained from the DCM-QGSM-SMM event generator. Anisotropic flow was calculated in the kinematic regions where the normalized (p_T, y) population is close to unity and uniform (blue rectangles for rapidity dependence and red rectangles for p_T dependence). They correspond to regions of the CBM acceptance where reconstruction and identification efficiency is close to being uniform and therefore no correction for (p_T, y) dependence of the reconstruction efficiency is needed in flow measurements. Measurement in wider kinematic regions will require efficiency corrections and is a subject of further studies. The slope of the directed



flow dv_1/dy at midrapidity is extracted by fitting the rapidity dependence of directed flow with a first order polynomial function at $y \in [-0.4, 0.4]$.

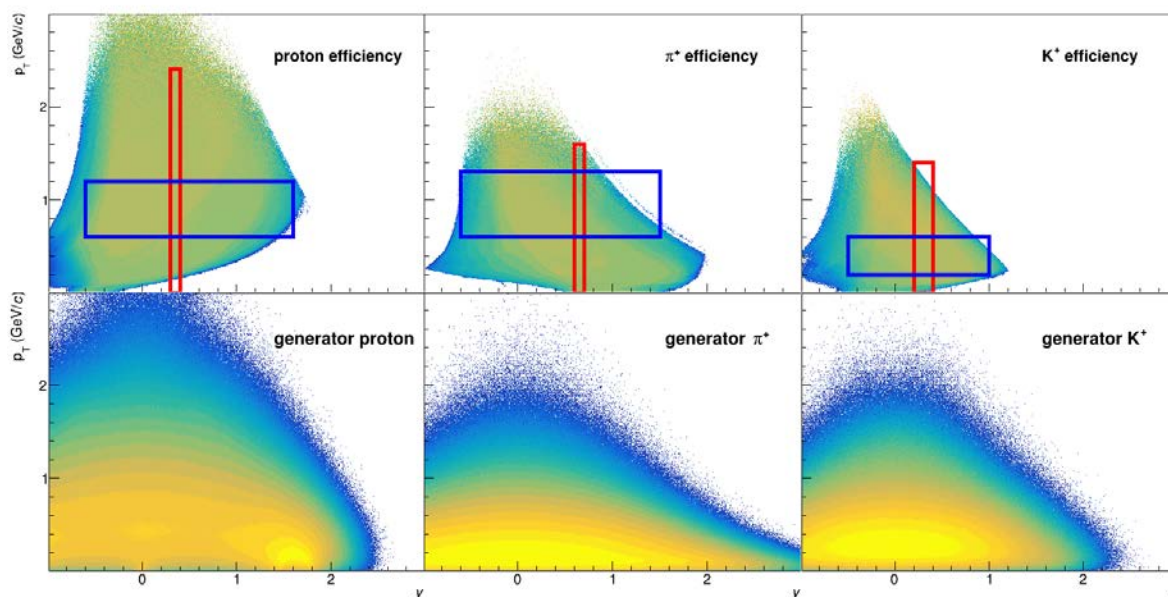
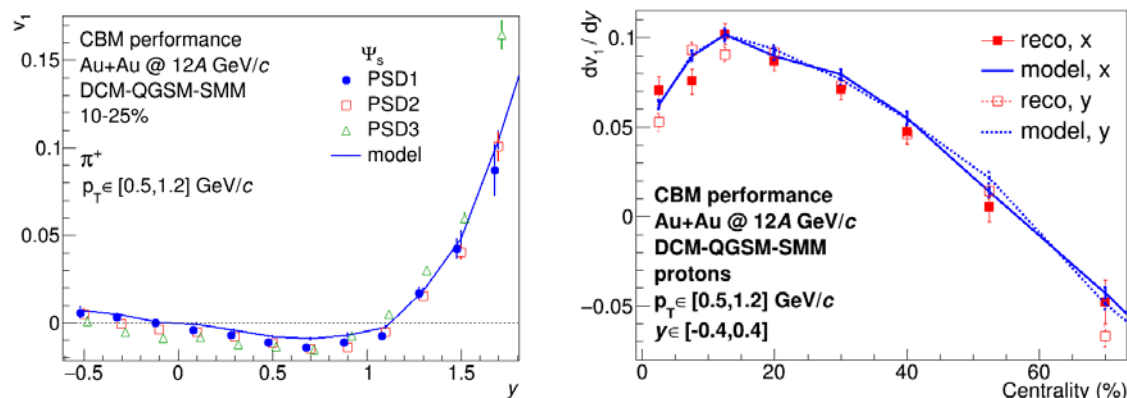


Figure 11. Acceptance & efficiency maps: proton, π^+ , and K^+ (details in text).

Figure 12 (left) presents the effect of choice of symmetry plane source on calculated values of proton directed flow. True dependencies are compared with calculations relative to symmetry planes reconstructed using different groups of PSD modules. One can see that with the shift to more peripheral modules for symmetry plane estimation (from PSD1 to PSD3) additional correlations arise at higher rapidity reducing the agreement of reconstructed flow values with the generator input. Figure 12 (right) shows the slope of proton directed flow at midrapidity, dv_1/dy , as a function of centrality. Since in the selected region of p_T and rapidity y ($p_T \in [0.5, 1.2]$, $y \in [-0.4, 0.4]$) the normalized population of the proton (see Fig. 11) is rather flat, even without applying efficiency corrections the v_1 slope at midrapidity at the generator level is well reproduced.



This project has received funding from the European Union's Horizon 2020 research and innovation programme under grant agreement No. 871072.

Figure 12. Left: Directed flow of protons as a function of rapidity extracted relative to symmetry plane estimates from PSD1, PSD2 and PSD3 subevents. Centrality 10-25%. Lines show the values obtained from the generator input. Right: Slope of proton directed flow dv_1/dy at midrapidity as a function of centrality. Blue lines show the generator-level results.

Figure 12 (left) shows the rapidity dependence of directed flow for positively charged kaons. Results are shown for the flow of generator-level particles calculated relative to the true reaction plane (blue line) and wrt. spectator symmetry plane estimated from different PSD subevents. It can be seen that additional correlations arise if the spectator plane is estimated using signals from outer PSD modules (PSD2 and PSD3 subevents) which are contaminated by the signal from produced particles. Figure 12 (right) presents the rapidity dependence of directed flow calculated relative to the true reaction plane for the tracks matched to generator-level positively charged kaons and tracks identified as kaons using time-of-flight information. This comparison reveals a significant effect on flow calculations due to impurity of the kaons selection in the backward region, where a fraction of tracks from protons and positive pions are passing the Bayesian selection criteria.

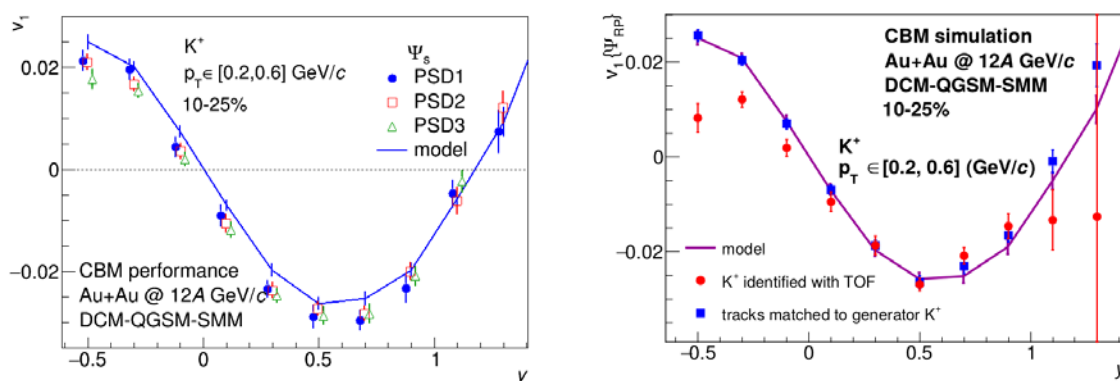


Figure 13. Directed flow of positively charged kaons as a function of rapidity. Results are for 10-25% centrality class. Left: Comparison of the v_1 at the generator-level with results relative to spectator symmetry plane estimates from different PSD subevents. Right: Comparison of the v_1 at the generator-level with results for tracks selected as K^+ .

2.4 Summary

Procedure for centrality determination based on charged hadron multiplicity is established for the CBM experiment at FAIR and implemented in the CentralityFramework software package [12]. Performance of the CBM experiment for measurements of the directed flow of protons and positively charged kaons with respect to the projectile spectator symmetry plane is investigated. The analysis is based on Au+Au collisions at the top SIS100 beam momentum of 12A GeV/c simulated with the DCM-QGSM-SMM event generator and transported through the CBM material using GEANT4 Monte-Carlo package. Results for v_1 are reported as a function of event centrality, particle transverse momentum and rapidity for Au+Au collisions at beam momentum of 12A GeV/c. A data-driven procedures for centrality determination, particle identification and symmetry plane reconstruction have been developed and used in the performance studies. Dependence of the results on the details of the



spectator symmetry plane estimation and purity of particle identification is studied by comparing the reconstructed signals with the event generator input. Additional correlations arise if the spectator plane is estimated using signals from outer PSD modules which are contaminated by the signal from produced particles. It is found that impurity of the kaon selection in the backward region, where a fraction of tracks from protons and positive pions are passing the Bayesian selection criteria has a significant effect on extracted flow signal.

3. Performance studies for the MPD experiment at NICA

The Nuclotron-based Ion Collider facility (NICA) is under construction at the Joint Institute for Nuclear Research (JINR), Dubna, Russia. NICA will collide heavy-ions (198Au + 198Au, 209Bi + 209Bi) at energies in the range of $\sqrt{s_{NN}} = 4$ to 11 GeV per nucleon pair in the center-of-mass system to provide an opportunity of studying the matter in the region of high net-baryon density [13]. The Multi-Purpose Detector (MPD) experiment at NICA will measure various prominent diagnostic probes sensitive to the Equation-of-State (EOS) and transport properties of the strongly interacting matter.

In this report, we discuss the anticipated performance of the MPD for the particle identification, centrality determination and anisotropic flow measurements of identified hadrons.

We used the cascade version of the Ultra-relativistic Quantum Molecular Dynamics (UrQMD) model (version 3.4) [8] to simulate the heavy-ion collisions at NICA energies: $\sqrt{s_{NN}} = 4.5, 7.7$ and 11 GeV. In total, the sample of 100 M of minimum bias Au + Au and Bi + Bi events was used to analyze the directed and elliptic flow signals of the identified hadrons. At the next step, the sample of UrQMD minimum bias events was made as an input for the full chain of realistic simulations of the MPD detector subsystems based on the GEANT4 [3] platform and reconstruction algorithms built in the MPDROOT. The resulting performance of the MPD has been verified by comparison of the results obtained from the analysis of these fully reconstructed events with the event generator input.

The MPD has been designed as a 4π spectrometer for detecting charged hadrons, electrons and photons in heavy-ion collisions at high luminosity. In the first stage of operation in 2023, the MPD will consist of the Time Projection Chamber (TPC), the Time-of-Flight (TOF) detector, the electromagnetic calorimeter (EMCal), the forward hadron calorimeter (FHCAL) and the fast forward detector (FFD); see left panel of Figure 14. The TPC will provide 3D tracking of charged particles, as well as measuring the specific ionization energy loss dE/dx to identify the particles with $\eta < 1.2$. The TPC will be surrounded by a cylindrical barrel of the Time-of-Flight (TOF) detector. The TOF system of the MPD developed to identify the charged hadrons is based on the technology of Multigap Resistive Plate Chambers (MRPC). The detector is designed to provide both the time and coordinate measurements with the accuracy of the order of 80 ps and 0.5 cm, respectively. Two arms of hadron calorimeters (FHCAL), made of 44 modules of lead-scintillator sampling calorimeters and covering the pseudorapidity range of $2.0 < \eta < 5$, will measure the forward going energy distribution. The information from FHCAL about the energy deposit will be used to reconstruct the event plane, see right panel of Figure 14.



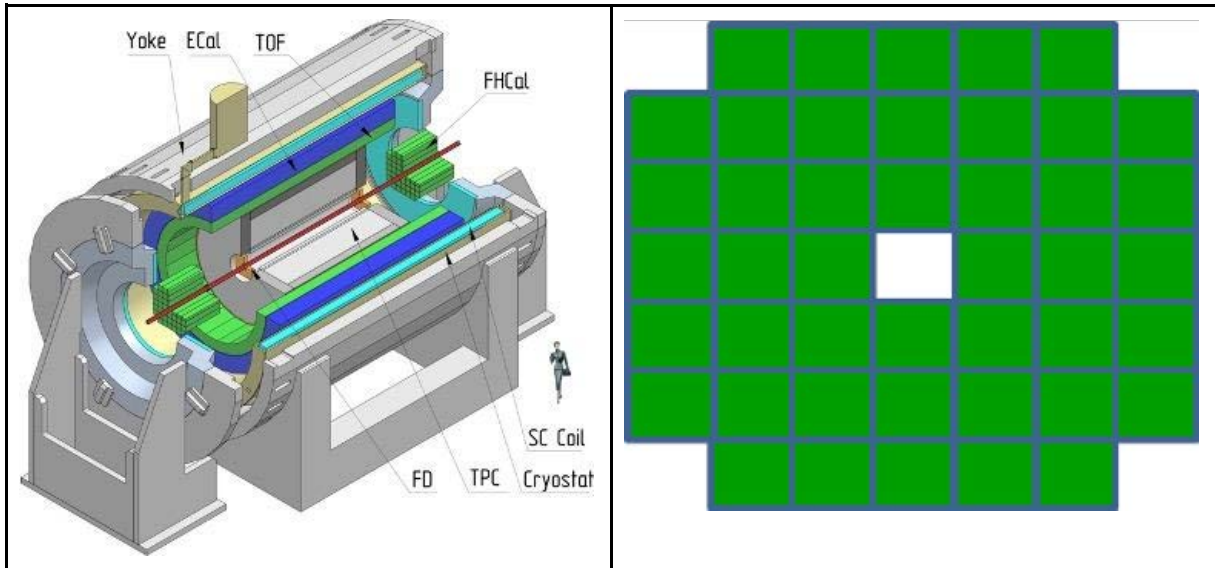
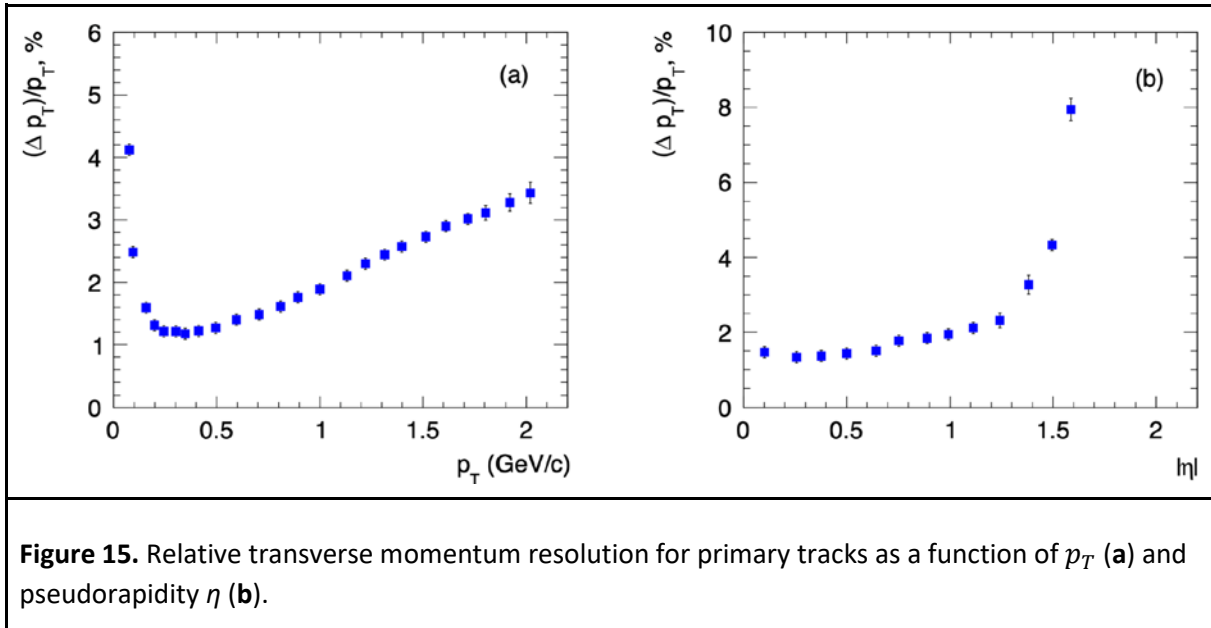


Figure 14. (left) The schematic view of the Multi-Purpose Detector (MPD) detector in Stage 1 (right). The module structure of the forward hadron calorimeter (FHCAL) calorimeter (front view).

3.1 Procedure for charged hadron identification in the MPD experiment

The track reconstruction in MPD is based on the Kalman filter technique [14] and the minimal requirement of 16 TPC hits ensures a low momentum error. We introduced a 3D distance of the closest approach (DCA) between the track and the reconstructed primary vertex. The primary tracks were selected with the 2σ cut on the DCA. The relative transverse momentum resolution ($\Delta p_T/p_T$) for primary tracks as a function of p_T is shown in the left panel of Figure 15. $\Delta p_T/p_T$ is less than 3% for tracks with $0.1 < p_T < 1.8$ GeV/c and for the pseudorapidity range $|\eta| < 1.5$, see right panel of Figure 15. The resolution degrades rapidly above $\eta = 1.5$ due to the decrease of the number of TPC space points. The analysis was performed for tracks from the kinematic regions of TPC with the higher tracking efficiency: $0.2 < p_T < 2.5$ GeV/c and $|\eta| < 1.5$.





Identification of the charged hadrons in the MPD experiment is based on a combination of momentum information, the specific energy loss (dE/dx) in the Time-Projection Chamber (TPC) and time-of-flight measurements from the TOF detector. Time-of-flight measurements from the TOF detector were used in conjunction with the measured particle momentum and flight-path length to generate a mass-squared (m^2) distribution, see left panel of Figure 16.

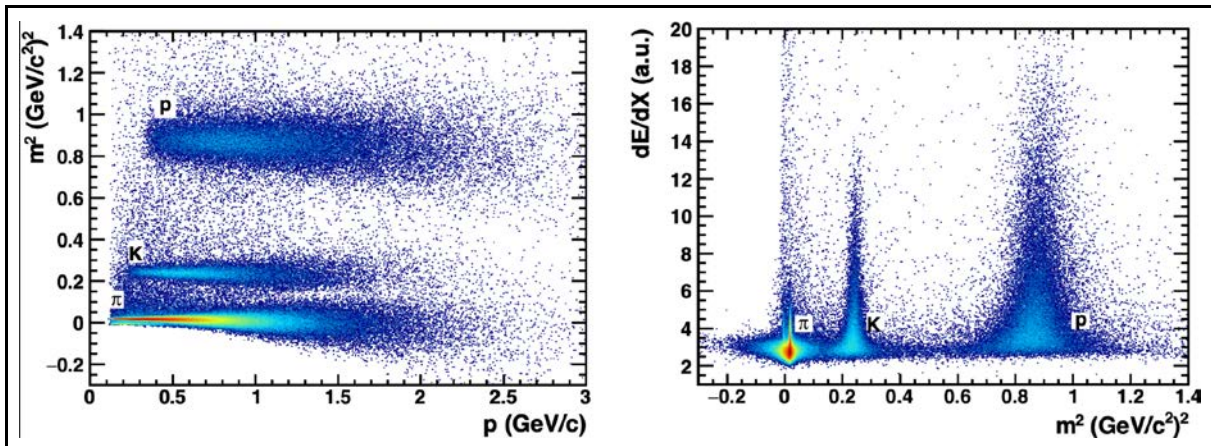


Figure 16. (left) Momentum dependence of mass-squared (m^2) of charged particles. (right) dE/dx vs. m^2 for combined system Time-Projection Chamber (TPC) + Time-of-Flight (TOF) for charged hadrons with momentum $0 < p < 3$ GeV/c.

The identified candidates (hadrons and light nuclei) can be selected within the pre-defined elliptical ranges around a nominal position in dE/dx and m^2 axes fixed for each type of particles, see right panel of Figure 16. The widths of these distributions provide an additional criterion of identification. Charged pions and kaons can be easily distinguished up to 1.5 GeV/c in transverse momentum,

whereas at higher momenta, the particle species start to significantly overlap. Protons and mesons can be separated up to 2.5 GeV/c.

3.2 Methods for centrality determination based on charged particle multiplicity.

The size and evolution of the matter created in relativistic heavy-ion collisions strongly depend on collision geometry, defined by the impact parameter. However, the impact parameter (b) cannot be measured directly in an experiment but might be inferred from final state observables using the centrality procedure. Experimental heavy-ion collisions can be characterized by the measured particle multiplicities N_{ch} around midrapidity (or the total transverse energy) or by the energy E_{sp} measured in the forward rapidity region, which is sensitive to the spectator fragments. The measured dN/dN_{ch} (dE/dE_{sp}) distribution is divided into percentile centrality classes, with the most central class defined by X% of events with the highest value of N_{ch} (smallest forward energy E_{sp}), which corresponds to small values of the impact parameter b . This is referred to as 0–X% centrality. The correlation between measured N_{ch} (E_{sp}) and b of the collision is then inferred by fitting a specific model of the collision dynamics to experimental data. Then this model is used to extract information about b . Experiments at high energies usually employ the Monte-Carlo Glauber (MC-Glauber) approach [7, 9], see Section 2.2 of the report for the details and implementation for the CBM.

While this approach offers a convenient parametrization of the measured distributions, it may suffer from systematic uncertainties, and limitations of the Glauber model [15]. At lower energies (relevant to the FAIR-NICA program), the spectator-participant paradigm becomes less justified. Recently, a new method for reconstructing the impact parameter b distributions from the measured N_{ch} was proposed [16,17]. The Γ -fit method is based on the assumption that the relation between the measured N_{ch} and b is purely probabilistic and can be inferred from data without relying on any specific model of collisions. This typical inverse problem can be solved by a deconvolution method. A gamma distribution is used for the fluctuation kernel $P(N_{ch} | b)$ to model fluctuations of N_{ch} at a fixed impact parameter. The parameters of the gamma distribution were then extracted by fitting the measured distribution of N_{ch} .

In this report, we present the procedure of centrality determination for the Multi-Purpose Detector at NICA and its performance using the multiplicity of produced charged particles at midrapidity. In order to reconstruct the impact parameter distribution, the MC- Glauber approach and Γ -fit method have been employed. In total, the sample of 1 M minimum bias Au + Au events has been generated by UrQMD model [8] for the collision energies: $\sqrt{s_{NN}} = 4.5, 7.7, \text{ and } 11.5$ GeV. The selected collision energies can be used in the future for the direct comparison of the first MPD results with published results from the Beam Energy Scan program of the STAR experiment at RHIC [18]. The centrality definition in the STAR experiment is based on the measured charged particle multiplicity from the Time Projection Chamber (TPC) within pseudorapidity $|\eta| < 0.5$, uncorrected for detection efficiencies. We have applied the same acceptance cuts in our analysis. As an example, Figure 17 shows the charged particle multiplicity distribution for Au + Au collisions at $\sqrt{s_{NN}} = 7.7$ GeV obtained from the analysis of events from the UrQMD model (open squares).



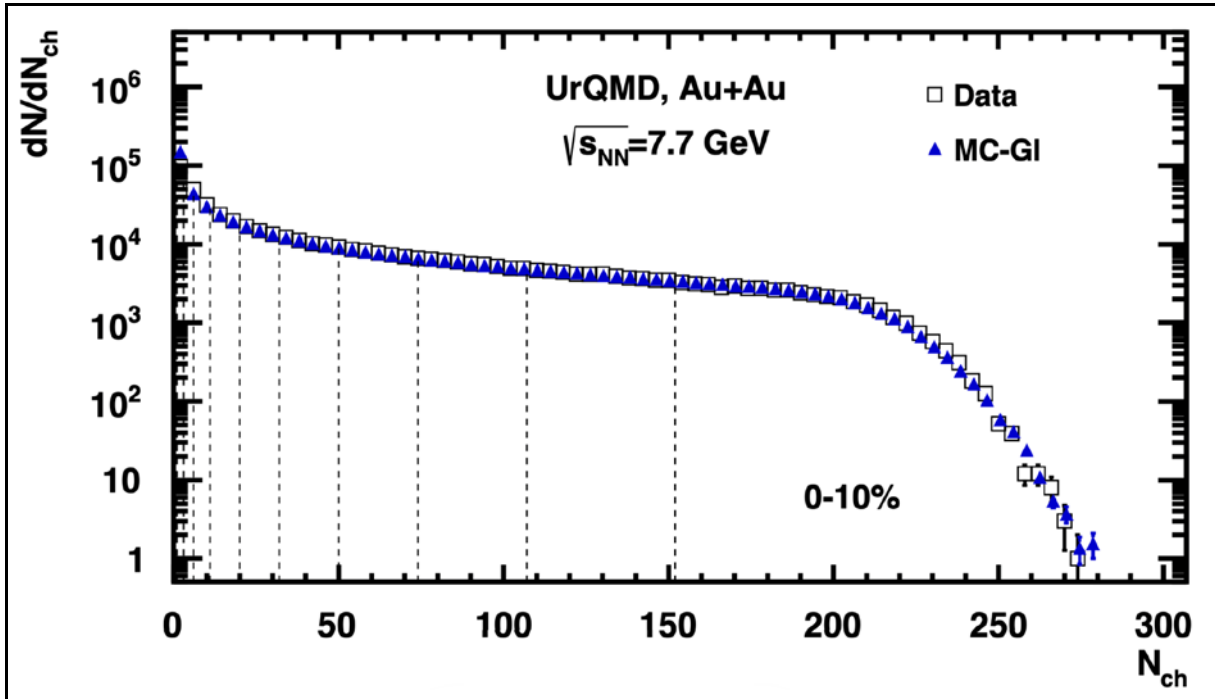


Figure 17. Charged particle multiplicity distribution from the UrQMD model (open squares) for Au + Au collisions at $\sqrt{s_{NN}}=7.7$ GeV compared to the fitted distribution using MC-Glauber (blue solid triangles). 10% centrality classes defined with MC-Glauber normalization are indicated with black dotted vertical lines.

3.2.1 Centrality determination using MC-Glauber method

The details for the procedure for centrality determination based on the MC-Glauber method is presented in the CBM part of the report, see section 2.2. Here we only briefly discuss the usage of the CentralityFramework software package [12] for the MPD simulated data.

- 1) In order to get MC-Glauber Au+Au events for each collision energy we used the 3.2 version of the PHOBOS MC-Glauber approach [19]. Two nucleons from different nuclei are assumed to collide if the relative transverse distance d between centers is less than the distance corresponding to the inelastic nucleon-nucleon cross section: $d < \sigma^{\text{inel}}/\pi$. For selected energies, the values of σ^{inel} are set to 29.3, 29.7, and 31.2 mb for $\sqrt{s_{NN}}= 4.5, 7.7,$ and 11.5 GeV, correspondingly [19].
- 2) The MC-Glauber defines the corresponding number of participating nucleons (N_{part}) and the number of binary nucleon-nucleon collisions (N_{coll}) for an event with a given impact parameter b . The multiplicity of a heavy-ion collision $M_{\text{MC-GI}}(N_a, f, \mu, k)$ is modeled as a sum of particles produced from a set of N_a independent emitting sources (“ancestors”), see Section 2.2. Each ancestor produces particles according to a negative binomial distribution



(NBD) $P_{\mu,k}$ with mean multiplicity per ancestor μ and width parameter k .

- 3) The track multiplicity distribution M_{MC-Gl} for the charged particles in TPC is simulated for an ensemble of events and various values of the NBD parameters μ , k , and the N_a parameter f . A minimization procedure is applied to find the optimal set of parameters that result in the smallest fitting criteria χ^2 .

As an example, Figure 17 shows the charged particle multiplicity distribution (open squares) with the MC-Glauber fit function (blue solid triangles). With the final set of parameters (f, μ, k) , the mean value of impact parameter b can be extracted for the centrality classes defined by the sharp cuts in the multiplicity distribution—see the dotted vertical lines in Figure 17.

3.2.2 Centrality determination using inverse Bayesian method (Γ -fit method)

The Γ -fit method [16,17] is based on the assumption that the relation between the measured N_{ch} and impact parameter b is purely probabilistic and can be inferred from the experimental data without relying on any specific model of collisions. The measured multiplicity distribution, $P(N_{ch})$, is obtained by summing the contributions to multiplicity at all impact parameters:

$$\frac{1}{M} M_{\Gamma-fit} \equiv P(N_{ch}) = \int_0^\infty P(N_{ch}|b)P(b)db = \int_0^\infty P(N_{ch}|c_b)dc_b, \quad (19)$$

where $P(b)$ is the probability distribution of the impact parameter and c_b denotes the centrality, defined as the cumulative distribution of the impact parameter: $c_b \equiv \int^b P(b')db'$. $1/M$ denotes that the distribution is normalized $\int P(N_{ch})dN_{ch}$. $P(N_{ch}|c_b) = P(N_{ch}|b)$ is the probability of N_{ch} at fixed b . The probability distribution $P(b)$ of b reads

$$M_{MC-Gl}(N_a, f, \mu, k) = \sum_{I=1}^{N_a(f)} P_{\mu,k}^I, \quad N_a(f) = fN_{part} + (1-f)N_{coll}. \quad (20)$$

where $P_{inel}(b)$ is the probability for an inelastic collision to occur at a given b , and σ_{inel} is the inelastic nucleus–nucleus cross section. The probability for an inelastic collision is close to 1 for non-peripheral collisions, and in this method of centrality determination, the approximation $P_{inel}(b) \sim 1$ is used. A gamma distribution is used for the fluctuation kernel $P(N_{ch}|b)$ to model the fluctuations of N_{ch} at a fixed impact parameter:

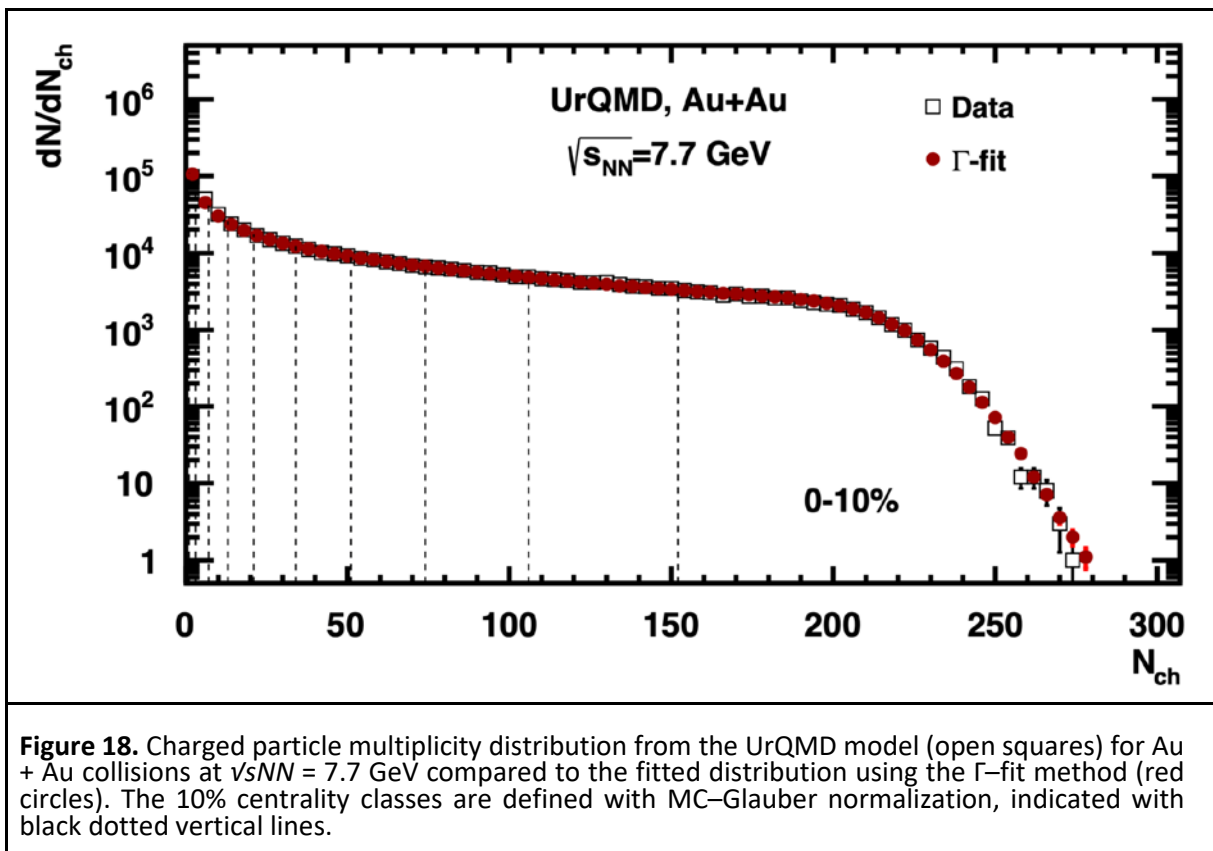
$$P(N_{ch}|b) = \frac{1}{\Gamma(k)\theta^k} N_{ch}^{k-1} e^{-N_{ch}/\theta}, \quad (21)$$

where k and ϑ are two positive parameters, which generally depend on c_b . They define the shape of the multiplicity distribution and can be attributed to the mean $\langle N_{ch} \rangle$ and standard deviation $\sigma_{N_{ch}}$ of the distribution: $\langle N_{ch} \rangle = k\vartheta$, $\sigma_{N_{ch}} = \sqrt{k\vartheta}$. One assumes that the mean N_{ch} is a smooth, monotonously decreasing function of c_b . To define the variable k , we used the following parameterization:



$$k(c_b) = k_0 \cdot \exp \left[- \sum_{i=1}^3 a_i (c_b)^i \right], \quad (22)$$

As a result, we have five fitting parameters ϑ , k_0 , and a_i . The parameters of the gamma distribution were then extracted by fitting the measured distribution of N_{ch} [16,17]. We then tested the procedure on the same charged particle multiplicity distribution from the UrQMD model for Au +Au collisions at $\sqrt{s_{NN}} = 7.7$ GeV—see Figure 18. The result of the fit is shown as red circles. The fit returns the parameters of the gamma distribution in Equation (22), which allows us to reconstruct the probability of N_{ch} at fixed centrality c_b . The probability distribution of impact parameter, b , at fixed N_{ch} , can be obtained by Bayes' theorem: $P(b/N_{ch}) = P(N_{ch}/b)P(b)/P(N_{ch})$, where $P(N_{ch}/b) = P(N_{ch}/c_b)$ is given by Equation (22) and $c_b \sim \pi b^2/\sigma_{inel}$ [16, 17].

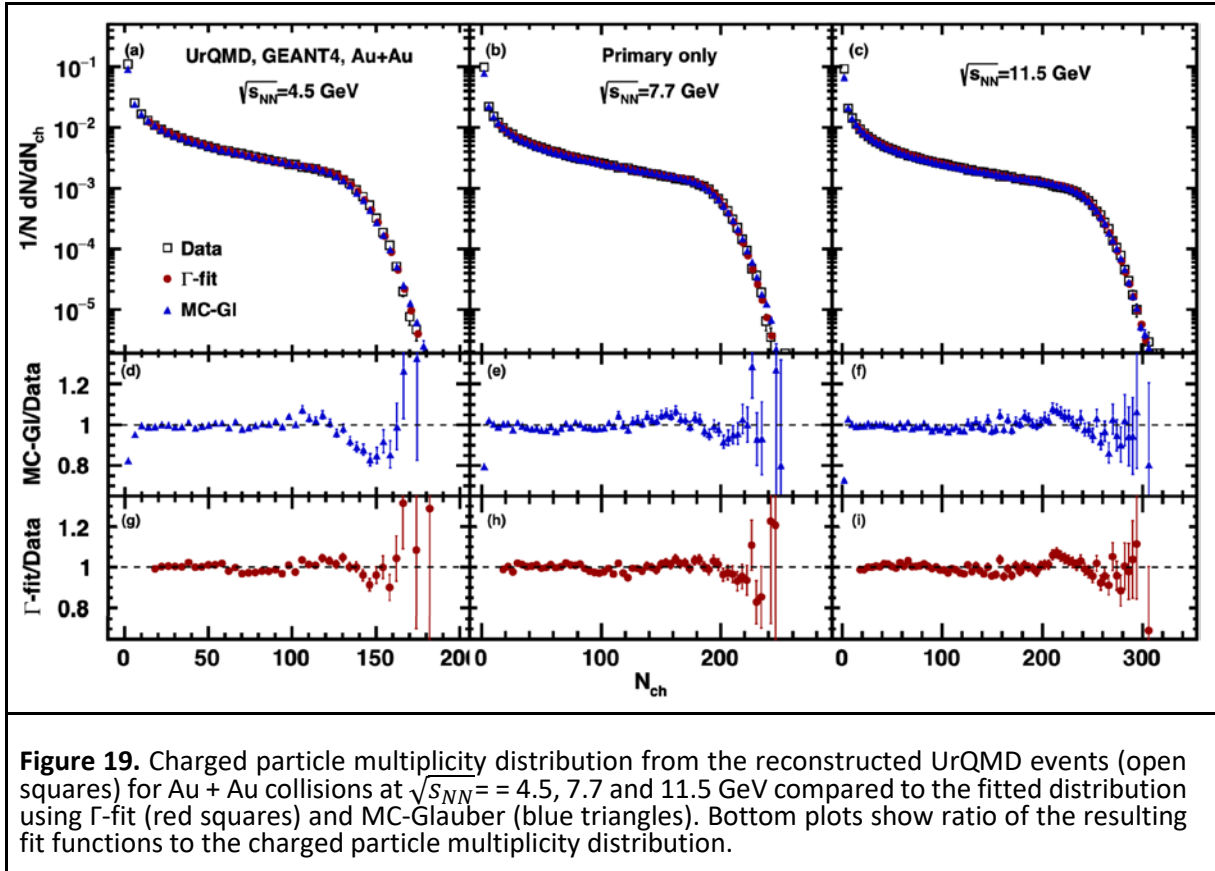


3.2.3 The comparison of the methods

At the next step of the analysis, the sample of UrQMD minimum bias events was made as an input for the full chain of realistic simulations of the MPD detector subsystems based on the GEANT4 platform and reconstruction algorithms built in the MPDROOT framework. The track reconstruction in MPD is based on the Kalman filter technique, and the minimal requirement of 16 TPC hits ensures a low momentum error. We have introduced a 3D distance of the closest approach (DCA) between



the track and the reconstructed primary vertex. The primary tracks have been selected with the 2σ cut on the DCA. Figure 19 shows the multiplicity distributions for Au + Au collisions at $\sqrt{s_{NN}} = 4.5, 7.7$ and 11 GeV obtained from fully reconstructed UrQMD events (open squares).



Red circles show the result of the fitting procedure for Γ -fit and blue triangles for the MC-Glauber methods. The fits were carried out for multiplicities in the range of $N_{ch} > 15$. The bottom parts of Figure 19 show the ratio of the track multiplicity distribution to the corresponding fit. The ratio plots show that both methods can reproduce the charged particle multiplicity distribution with good accuracy. Figures 20 and 21 show the resulting centrality dependence of the mean impact parameter b . Results are compared with b extracted directly from the corresponding models. It is shown that values of b reconstructed by both methods are in good agreement with the one from the models. Results for the Γ -fit approach tend to be in a better agreement. However, it should be noted that this approach requires the total integral of the multiplicity distribution to be evaluated separately. Thus, Γ -fit method is more sensitive to any bias, such as trigger inefficiencies, that could distort the estimation of the total integral of the multiplicity distribution.

Secondary particles produced during the particle propagation through the MPD detector introduce a bias in the correlation between the impact parameter and charged particle multiplicity. It is clearly seen from the comparison of the results from the reconstructed data with primary track selection (Figures 20 and 21) and results from the direct analysis of UrQMD model events.



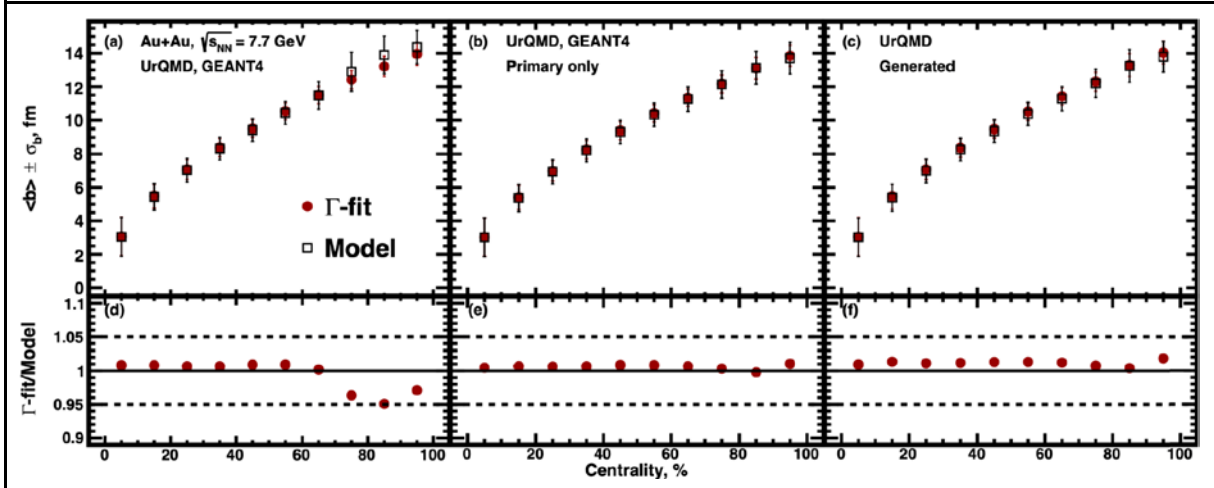


Figure 20. Centrality dependence of the average impact parameter (b) for Au + Au collisions at $\sqrt{s_{NN}} = 7.7$ GeV for Γ -fit approach. Multiplicity of charged particles were gathered for (a) all charged tracks and (b) only primary tracks from the model itself. Additional track quality cut $N_{hits} > 16$ was applied. The resulting values were compared with generated UrQMD data without any reconstruction (c). Lower plots show the fit-to-model ratio.

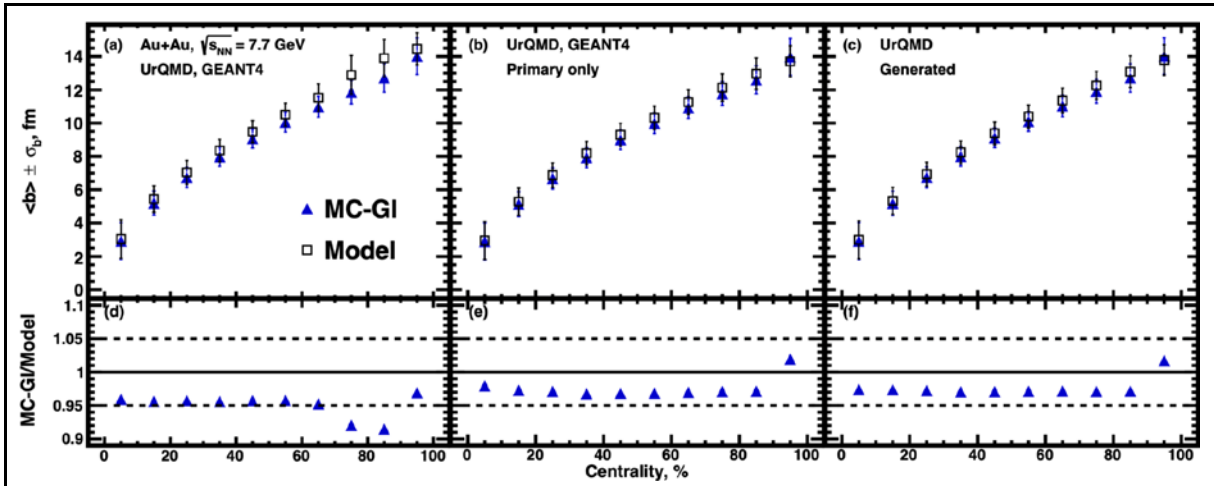


Figure 21. Centrality dependence of the average impact parameter (b) for Au + Au collisions at $\sqrt{s_{NN}} = 7.7$ GeV for MC-Glauber approach. Multiplicity of charged particles were gathered for (a) all charged tracks and (b) only primary tracks from the model itself. Additional track quality cut $N_{hits} > 16$ was applied. The resulting values were compared with generated UrQMD data without any reconstruction (c). Lower plots show the fit-to-model ratio.

The systematic uncertainties with regard to the mean values of impact parameter b were obtained by independently varying the parameters of the initial parameters in each method. The fit procedures were repeated for all parameter variations. For the Γ -fit method, geometric inelastic nucleus–nucleus cross section σ^{inel} fit ranges were varied. σ^{inel} was varied within 2% from its value, and $N_{ch} > 10, 25, 30$ fit ranges were chosen. For the MC-Glauber approach, these parameters were a cross section of inelastic nucleon–nucleon collisions σ^{inel} (varied within 10%), radius R (varying within 0.04 fm) and



skin thickness a (varying within 0.1 fm) of the nucleus, fit ranges ($N_{ch} > 10, 40$) and definition of the number of ancestors N_a . All values of the parameters are shown in the legend in Figure 22. It is shown that differences in the resulting impact parameter due to parameter variations are within 2–3%.

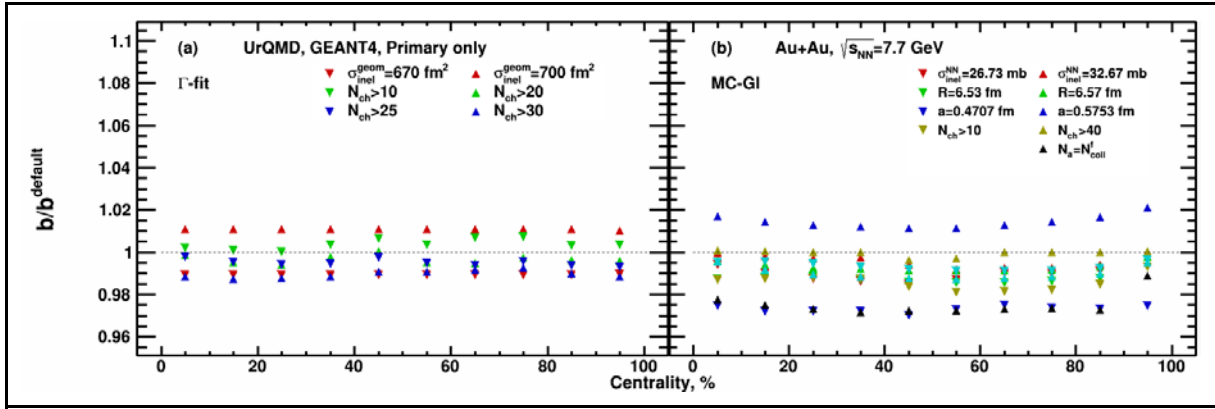


Figure 22. Sensitivity of the impact parameter b/b^{default} reconstruction to variations of parameters for the MC-Glauber and Γ -fit approaches as a function of centrality.

3.3 Performance for anisotropic flow measurement in the MPD experiment

Performance of the Compressed Baryonic Matter (MPD) experiment for the measurement of directed (v_1) and elliptic (v_2) flow of identified hadrons is presented as a function of collision centrality, particle transverse momentum and rapidity. In this work, we used the cascade version of the Ultra-relativistic Quantum Molecular Dynamics (UrQMD) model (version 3.4) [8] to simulate the heavy-ion collisions at NICA energies: $\sqrt{s_{NN}}=4.5, 7.7$ and 11 GeV. In total, the sample of 100 M of minimum bias Au + Au and Bi + Bi events was used to analyze the directed and elliptic flow signals of the identified hadrons. We applied the term “true” for these v_1 and v_2 results, obtained from the direct analysis of the generated events. At the next step, the same sample of UrQMD minimum bias events was made as an input for the full chain of realistic simulations of the MPD detector subsystems based on the GEANT4 [3] platform and reconstruction algorithms built in the MPDROOT. The v_n results obtained from the flow analysis of these fully reconstructed events are termed as the “reco” data.

The track reconstruction in MPD is based on the Kalman filter technique [18] and the minimal requirement of 16 TPC hits ensures a low momentum error. We introduced a 3D distance of the closest approach (DCA) between the track and the reconstructed primary vertex. The primary tracks were selected with the 2σ cut on the DCA. The centrality classes are defined based on the uncorrected charged particle multiplicity (N_{ch}) distribution in the TPC for pseudorapidity $|\eta| < 0.5$ and full azimuth. As an example, Figure 23 shows the track multiplicity distribution for the Au + Au (left panel) and Bi + Bi (right panel) collisions at $\sqrt{s_{NN}} = 7.7$ GeV compared to those from Monte Carlo



(MC)–Glauber simulations (red line) [19](see Section 3.2 for the details); 10% centrality classes are indicated with black vertical lines in the Figure 23.

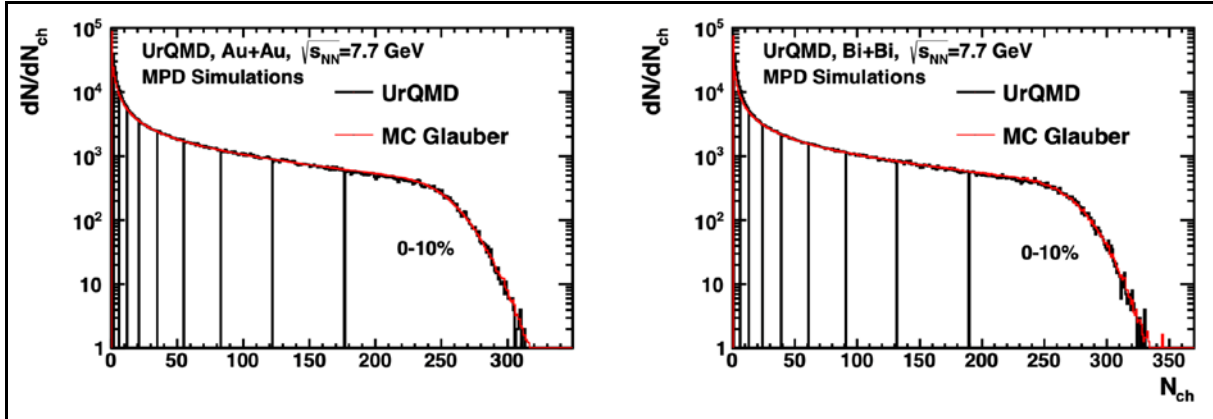


Figure 23. Track multiplicity distribution from the fully reconstructed Ultra-relativistic Quantum Molecular Dynamics (UrQMD) events for Au + Au (**left** panel) and Bi + Bi (**right** panel) collisions at $\sqrt{s_{NN}}=7.7$ GeV compared to the fitted distribution using Monte Carlo (MC)–Glauber approach (red line). The 10% centrality classes defined with MC–Glauber normalization are indicated with black vertical lines.

Identification of the charged hadrons in the MPD experiment is based on a combination of momentum information, the specific energy loss (dE/dx) in the Time-Projection Chamber (TPC) and time-of-flight measurements from the TOF detector, see section 3.1 for the details.

The identified candidates (hadrons and light nuclei) can be selected within the pre-defined elliptical ranges around a nominal position in dE/dx and m^2 axes fixed for each type of particles, see right panel of Figure 4. The widths of these distributions provide an additional criterion of identification. Charged pions and kaons can be easily distinguished up to 1.5 GeV/c in transverse momentum, whereas at higher momenta, the particle species start to significantly overlap. Protons and mesons can be separated up to 2.5 GeV/c. Short-lived weakly-decaying particles, such as K^0 and Λ , have been reconstructed using the invariant mass technique. The combinatorial background from uncorrelated particles has been reduced by the selection criteria based on the topology of the specific decay. The topological information about the primary and secondary decay vertex positions, the distance of the closest approach (dca) of the daughter particles to the primary vertex, the dca of the mother particle to the primary vertex, and the dca between the daughter tracks have been obtained by the Kalman filtering algorithm. The cuts have been applied to optimize the signal of K_S^0 and Λ particles.

The event plane method is used to obtain the present results for the directed (v_1) and elliptic (v_2) flow coefficients of the produced particles. The event plane method correlates the azimuthal angle ϕ of each particle with the azimuthal angle Ψ_n of the event plane determined from the anisotropic flow itself. Directed flow v_1 is large at NICA energies compared to other flow harmonics. It is the strongest in the forward rapidity region (i.e., in FHCAL acceptance area: $2 < |\eta| < 5$). For these reasons the first harmonic event plane $\Psi_{1,\text{FHCAL}}$ is used to study the present flow performance. The event plane angle



$\Psi_{1,\text{FHCaI}}$ has been calculated from the energy deposition in a given module of the FHCaI by constructing the so-called flow Q -vector $Q_{1,\text{FHCaI}}$ (two-dimensional vector in the transverse to the beam plane):

$$Q_{1,x} = \frac{\sum E_i \cos \varphi_i}{E_i}, \quad Q_{1,y} = \frac{\sum E_i \sin \varphi_i}{E_i}, \quad \Psi_{1,\text{FHCaI}} = \tan^{-1} \frac{Q_{1,y}}{Q_{1,x}}, \quad (23)$$

where φ_i is the azimuthal angle of the center of the i th FHCaI module in the transverse plane, and E_i is the energy deposition in the i th module of FHCaI (weight to improve the event plane resolution). The weights E_i have opposite signs for backward and forward rapidities due to the anti-symmetry of the v_1 as a function of rapidity y . The reconstructed $\Psi_{1,\text{FHCaI}}$ can be used to measure the differential directed flow $v_1^{\Psi_{1,\text{FHCaI}}}$ and elliptic $v_2^{\Psi_{1,\text{FHCaI}}}$ flow coefficients of the produced particles detected in TPC ($|\eta| < 1.5$).

$$v_n^{\Psi_{1,\text{FHCaI}}}(p_T, y, \text{centrality}) = \frac{\langle \cos(n(\varphi - \Psi_{1,\text{FHCaI}})) \rangle}{R_n(\Psi_{1,\text{FHCaI}})} \quad (24)$$

where $R_n(\Psi_{1,\text{FHCaI}})$ represents the event plane resolution factor. The two-subevent method with extrapolation algorithm was applied to estimate the event plane resolution factors. Figure 24 shows the centrality dependence of the event plane resolution factors $R_n(\Psi_{1,\text{FHCaI}})$ for directed v_1 (left panel) and elliptic v_2 (right panel) flow measurements for Au + Au collisions at $\sqrt{s_{NN}} = 4.5, 7.7$ and 11 GeV. For the mid-central Au + Au events at $\sqrt{s_{NN}} = 11$ GeV the resolution factor is as high as 0.9—for v_1 and 0.65—for v_2 measurements. The event plane resolution degrades slowly while decreasing the collision energy.

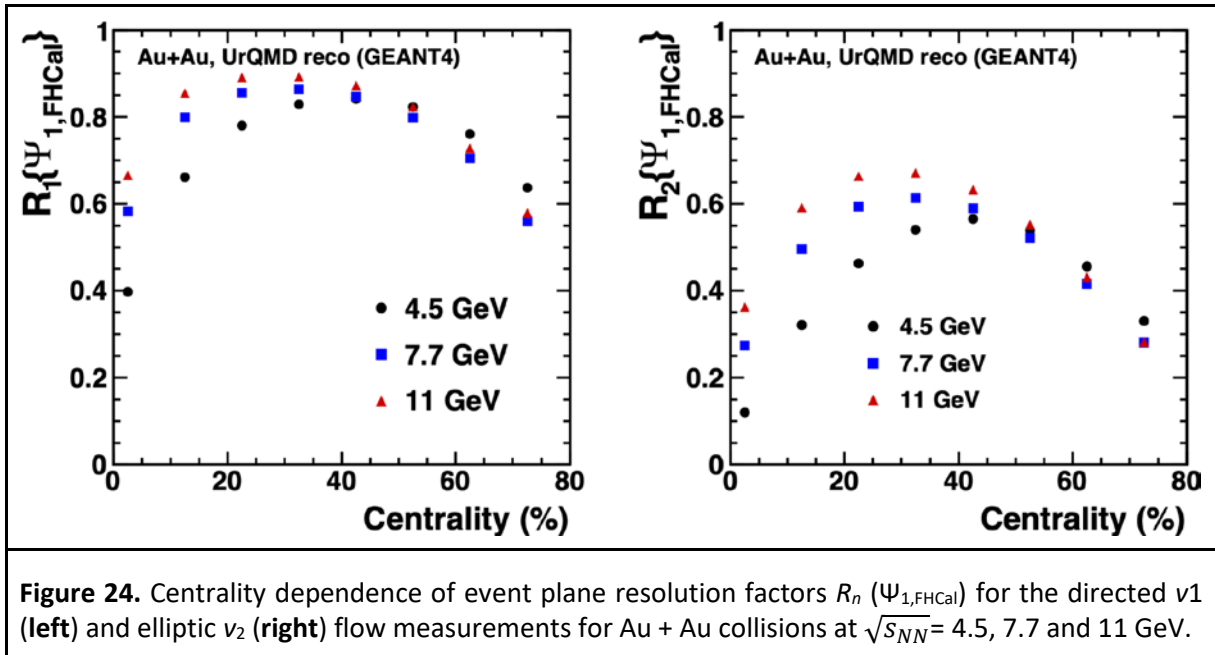
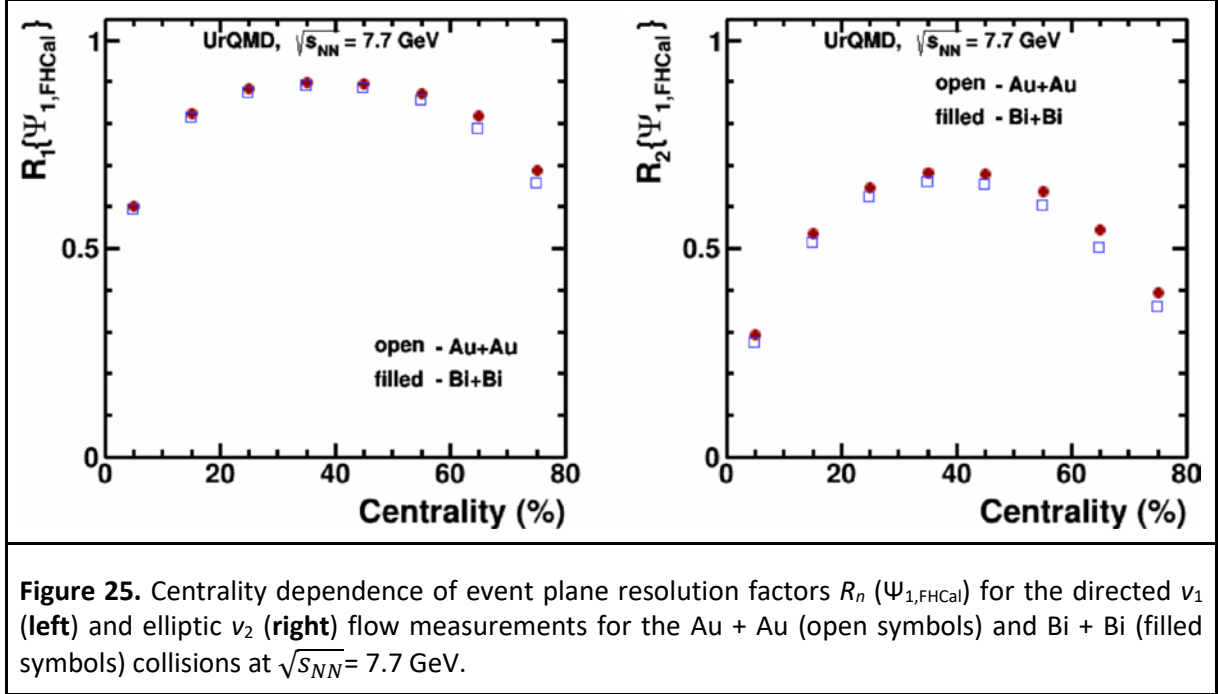


Figure 25 shows the comparison of the event plane resolution factors $R_n(\Psi_{1,\text{FHCaI}})$ for the Au + Au (open symbols) and Bi + Bi (filled symbols) collisions at $\sqrt{s_{\text{NN}}}=7.7$ GeV. As expected they have very similar values for the same bins in the collision centrality.

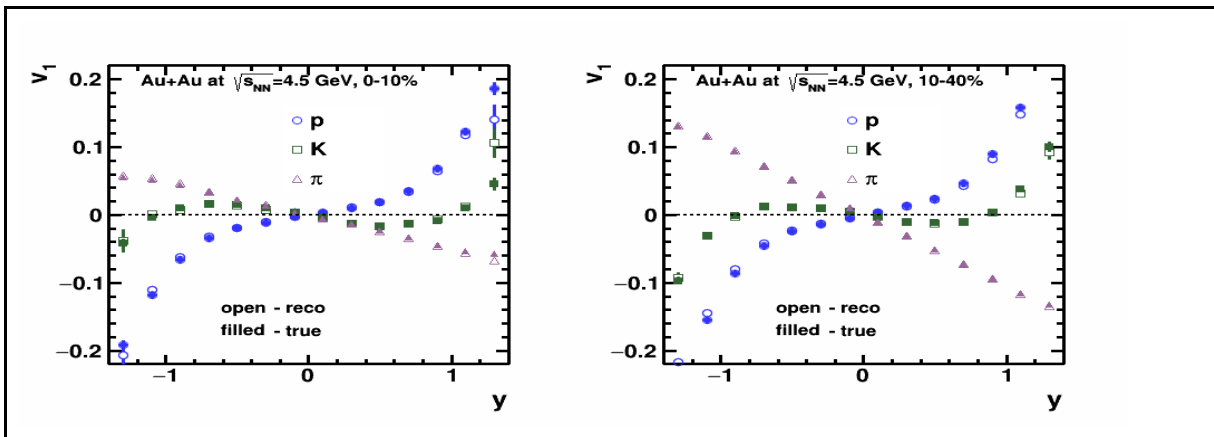
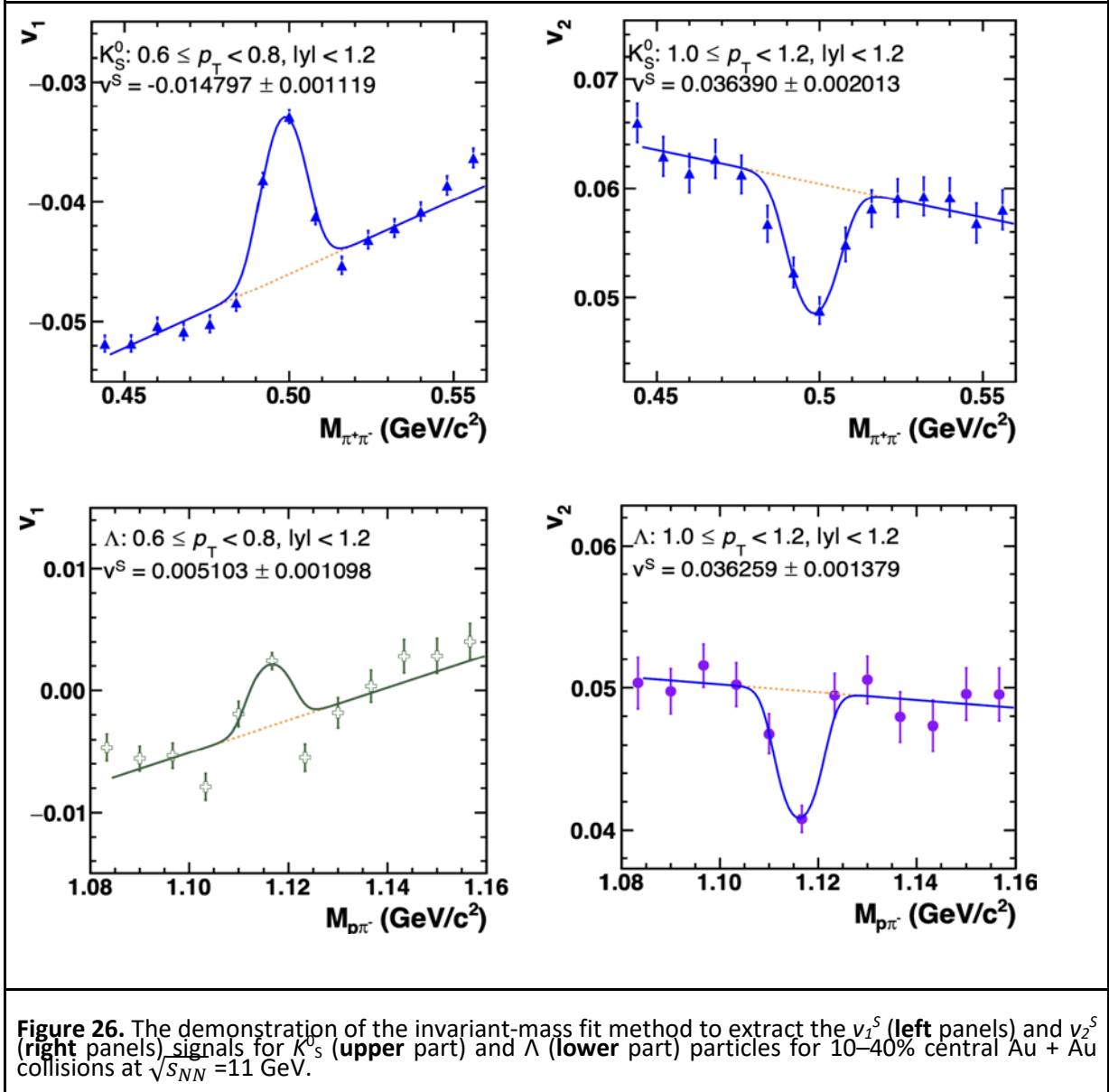


For V^0 particles, like K^0_s and Λ , the v_n^{SB} of the selected sample contains both v_n^S of the signal and the v_n^B of the combinatorial background. The invariant mass (M_{inv}) fit method was applied to extract the anisotropic flow values v_n^S for V^0 particles. Therefore, the $v_n^{SB} = \langle \cos[n(\phi^{\text{pair}} - \Psi_{1,\text{FHCaI}})] \rangle$ is measured as a function of invariant mass M_{inv} and p_T^{pair} :

$$v_n^{SB}(M_{\text{inv}}, p_T^{\text{pair}}) = v_n^S(p_T^{\text{pair}}) \frac{N^S(M_{\text{inv}}, p_T^{\text{pair}})}{N^{SB}(M_{\text{inv}}, p_T^{\text{pair}})} + v_n^B(p_T^{\text{pair}}) \frac{N^B(M_{\text{inv}}, p_T^{\text{pair}})}{N^{SB}(M_{\text{inv}}, p_T^{\text{pair}})}, \quad (25)$$

where $N^S(M_{\text{inv}}, p_T^{\text{pair}})$, $N^B(M_{\text{inv}}, p_T^{\text{pair}})$ and $N^{SB}(M_{\text{inv}}, p_T^{\text{pair}})$ are signal, background and total yields obtained for each p_T^{pair} interval from fits to the K^0_s and Λ invariant mass distributions, see Figure 26. Values for v_n^S signal for K^0_s and Λ particles were extracted via a direct fit to the $v_n^{SB}(M_{\text{inv}})$ for each p_T^{pair} selection by Equation (25).





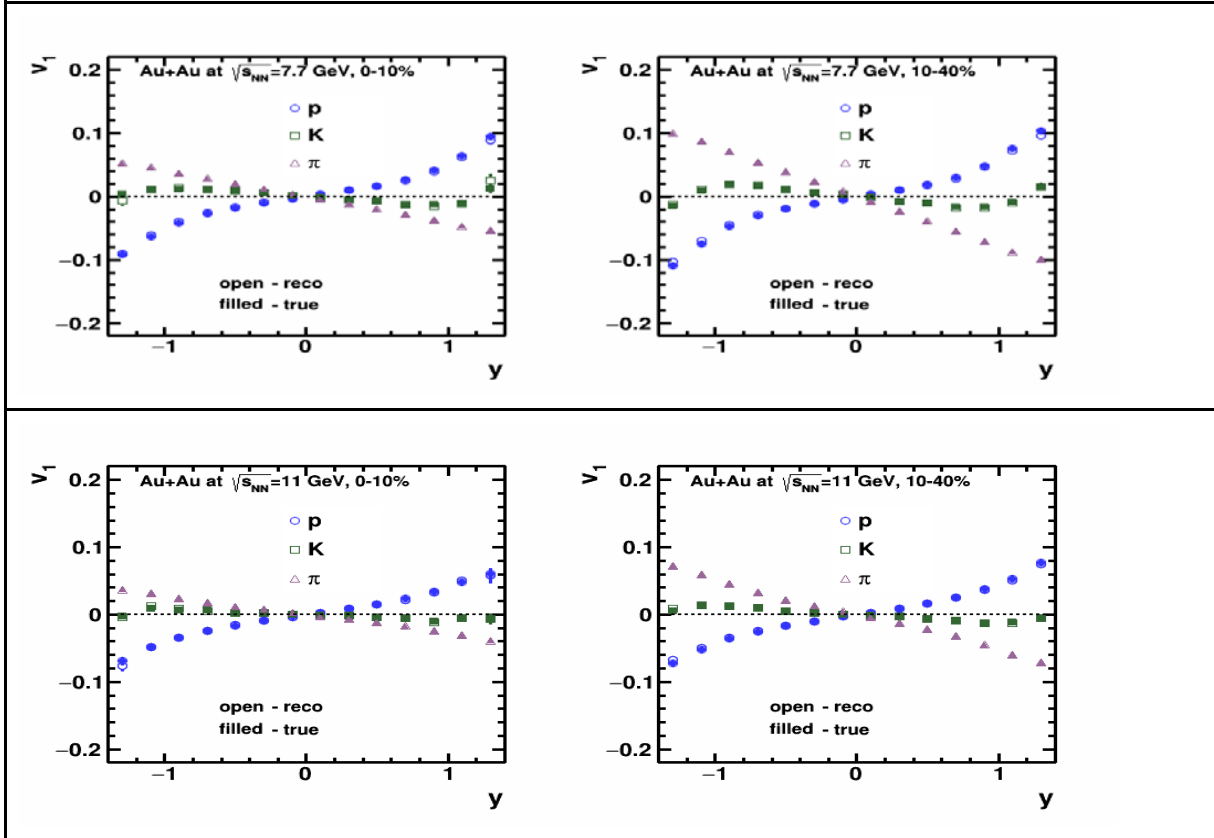


Figure 27. Rapidity y dependence of directed v_1 of charged pions, kaons and protons for 0–10% central (**left** panels) and 10–40% central (**right** panels) Au + Au collisions at $\sqrt{s_{NN}} = 4.5, 7.7$ and 11 GeV. The open symbols correspond to v_1 results from the analysis of the fully reconstructed events “reco” and closed symbols to the results from generated “true” UrQMD events.

That is, the background $v_n^B(M_{inv})$ was parametrized as a linear or quadratic function of p_T^{pair} selection) and v_n^S is taken as a fit parameter. The accuracy of the extraction procedure was verified by checking that the invariant mass (M_{inv}) dependencies of the sine coefficients $v_{sin,n}^{SB} = \langle \sin[n(\phi^{pair} - \Psi_{1,FHCal})] \rangle$, were all equal to zero within statistical errors. As an example, Figure 26 shows the demonstration of the invariant mass fit method to extract the v_1^S and v_2^S signals for K_s^0 (upper part) and Λ (lower part) particles for 10-40% central Au + Au collisions at $\sqrt{s_{NN}} = 11$ GeV.

The v_n results obtained by the event plane analysis can be affected by non-flow and flow fluctuations. The non-flow effects are mainly due to few particle correlations not associated with the reaction plane: Bose–Einstein correlations, resonance decays, momentum conservation and di-jets. In the present study, the large rapidity gap $|\Delta\eta| > 0.5$ between the particles detected in TPC and the particles in FHCal reduces the influence of possible non-flow contributions. The elliptic flow results $v^{\Psi_{1,FHCal}}$ obtained with respect to the spectator first-order event plane are expected to be less affected by the elliptic flow fluctuations because of the strong correlation between the $\Psi_{1,FHCal}$ and the true reaction plane Ψ_{RP} .



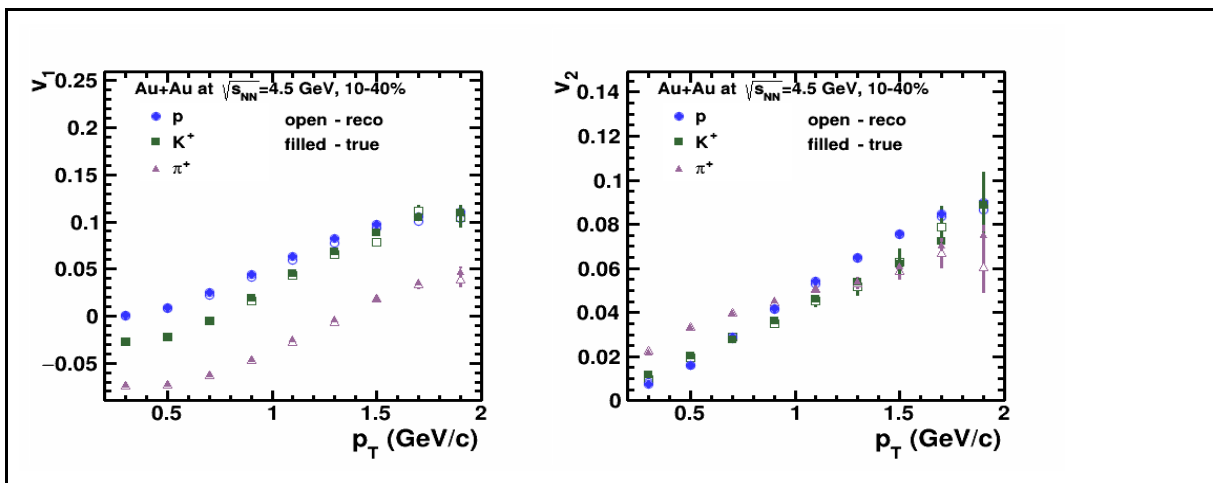
Figure 27 presents the rapidity dependence of directed $v_1(y)$ of charged pions, kaons and protons from Au +Au collisions at $\sqrt{s_{NN}} = 4.5, 7.7$ and 11 GeV. The left part of the Figure shows the results for 0–10% central collisions and right part for 10–40% central Au + Au collisions.

For all particle species, the directed flow crosses 0 at midrapidity. The reconstructed values “reco” of the directed flow are fully consistent with the generated “true” values in all centrality classes and collision energies. The v_1 and v_2 for identified charged hadrons as a function of transverse momentum p_T are presented in Figure 28 for 10–40% central Au + Au collisions at $\sqrt{s_{NN}} = 4.5, 7.7$ and 11 GeV.

The open symbols correspond to v_n results from the analysis of the fully reconstructed events “reco” and closed symbols and to the results from the generated “true” UrQMD events. The available statistics of 20 M minimum-bias events have allowed us to perform the detailed p_T -differential measurements of charged pions, kaons and protons up to 1.5 GeV/c. The more detailed p_T - differential studies as a function of centrality and rapidity will require a larger data sample of up to 300 M of minimum-bias events.

Figures 29 and 30 illustrate the MPD detector system performance for the differential directed $v_1(y)$ and elliptic flow measurements $v_2(p_T)$ of K^0_s and Λ particles for 10–40% central Au + Au collisions at $\sqrt{s_{NN}} = 11$ GeV. The results were obtained from the analysis of 25 M minimum-bias fully reconstructed UrQMD events. A good agreement is observed between the v_n results of K^0_s and Λ particles extracted by invariant-mass fit method illustrated in the Figure 26 from the fully reconstructed data “reco” and generated “true” UrQMD events.

The final part of this study is related to the comparison of the differential v_1 and v_2 results of identified hadrons from two colliding systems Au + Au and Bi + Bi at $\sqrt{s_{NN}} = 7.7$ GeV. The NICA collider is planned to start with first beams of ^{209}Bi ions in 2023. The delivery of ^{198}Au ions will be accomplished after this phase of NICA operation. Figure 31 presents the detailed comparison of the differential $v_1(y)$ results for charged pions and protons for 0–10% central (left panels) and 10–40% central (right panels) Au + Au and Bi + Bi collisions at $\sqrt{s_{NN}} = 7.7$ GeV. The $v_1(y)$ results have been obtained from the event plane analysis of 30 M fully reconstructed minimum-bias UrQMD events. The results received for Au + Au (Bi+ Bi) collisions are marked as open (filled) symbols. Figure 32 shows the performance of measuring the p_T dependence of directed v_1 (left) and elliptic v_2 (right) flow coefficients of charged pions and protons for 10–40% central Au + Au (open symbols) and Bi + Bi (filled symbols) collisions. The expected small difference is observed in the v_n results for two colliding systems.



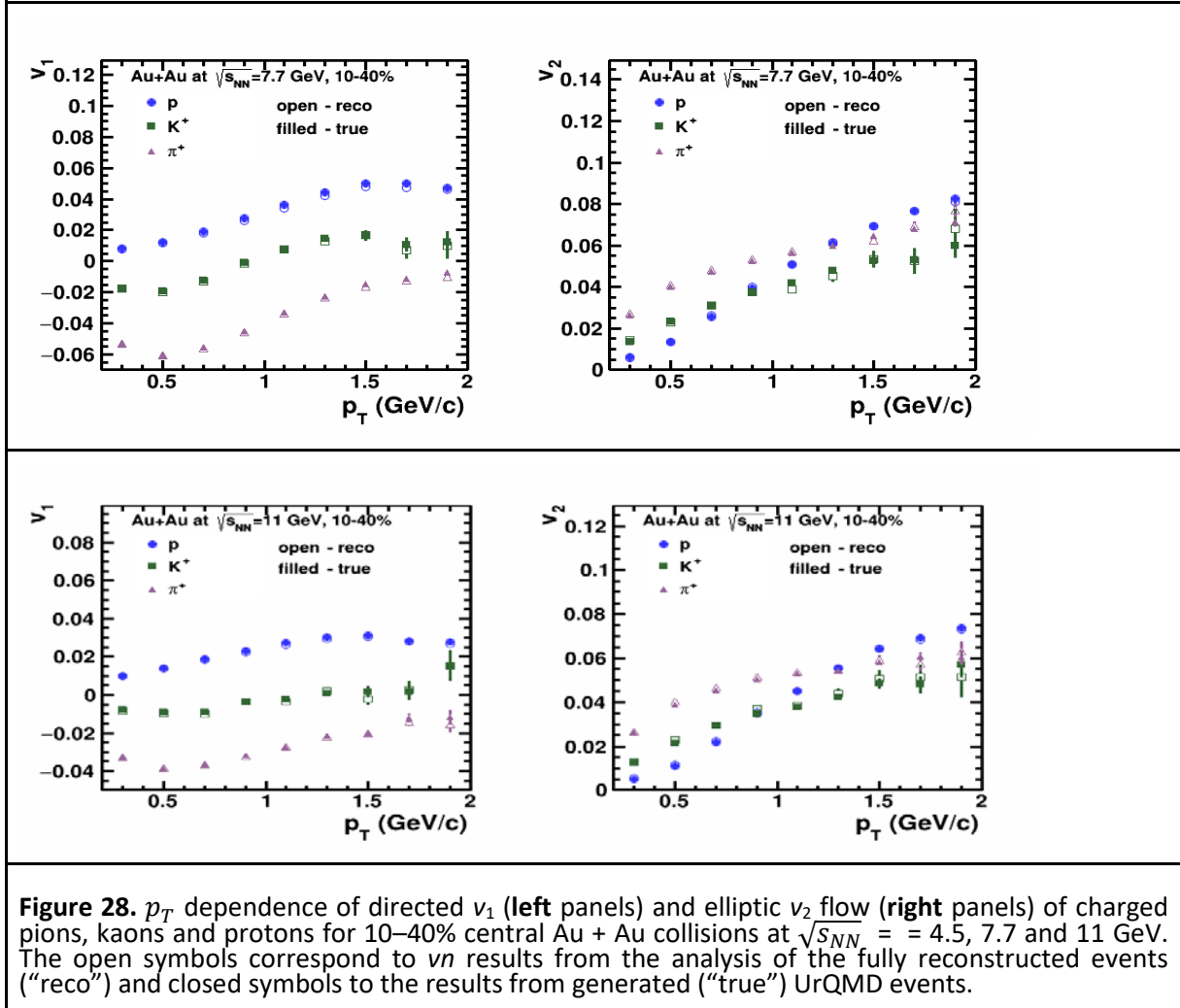


Figure 28. p_T dependence of directed v_1 (left panels) and elliptic v_2 flow (right panels) of charged pions, kaons and protons for 10–40% central Au + Au collisions at $\sqrt{s_{NN}} = 4.5, 7.7$ and 11 GeV. The open symbols correspond to vn results from the analysis of the fully reconstructed events ("reco") and closed symbols to the results from generated ("true") UrQMD events.

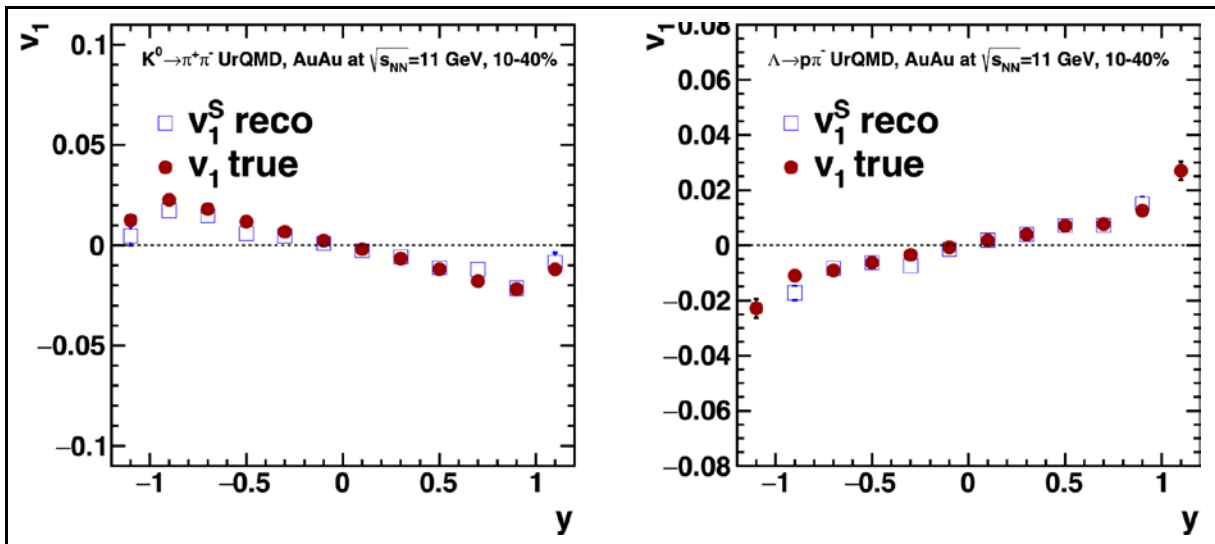


Figure 29. Rapidity y dependence of directed v_1 flow of K^0 (left) and Λ (right) particles for 10–40% central Au + Au collisions at $\sqrt{s_{NN}} = 11$ GeV: open symbols represents the "true" v_2 results and filled



symbols the “reco” v_2 results.

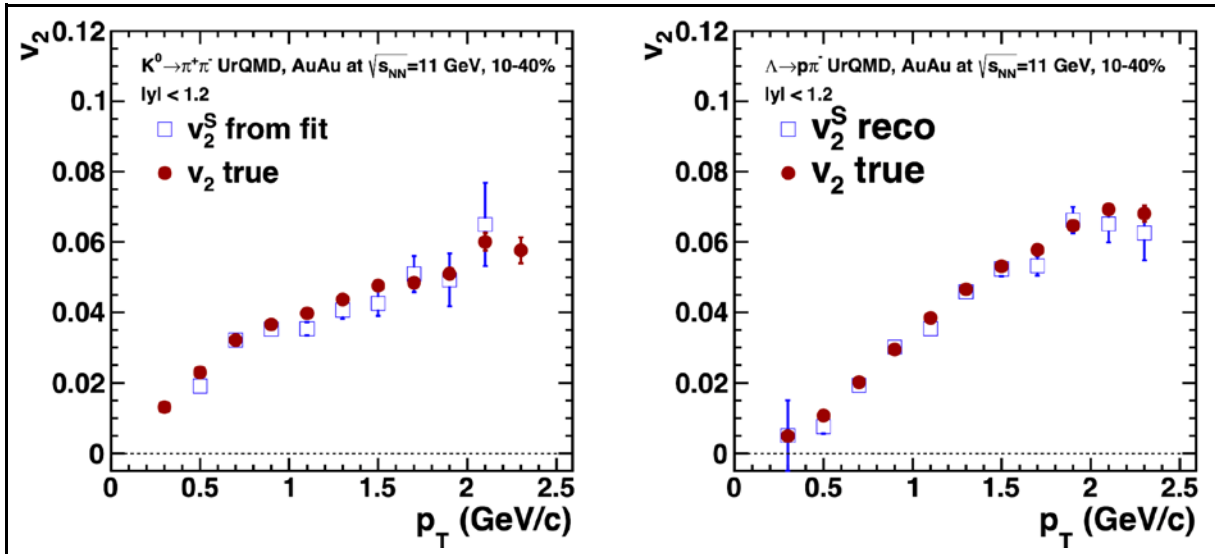


Figure 30. p_T dependence of $v_2(\Psi_{1,FHCal})$ of K^0_S (left) and Λ (right) particles for 10–40% central Au + Au collisions at $\sqrt{s_{NN}} = 11$ GeV: open symbols represent the “true” v_2 results and filled symbols the “reco” v_2 results.

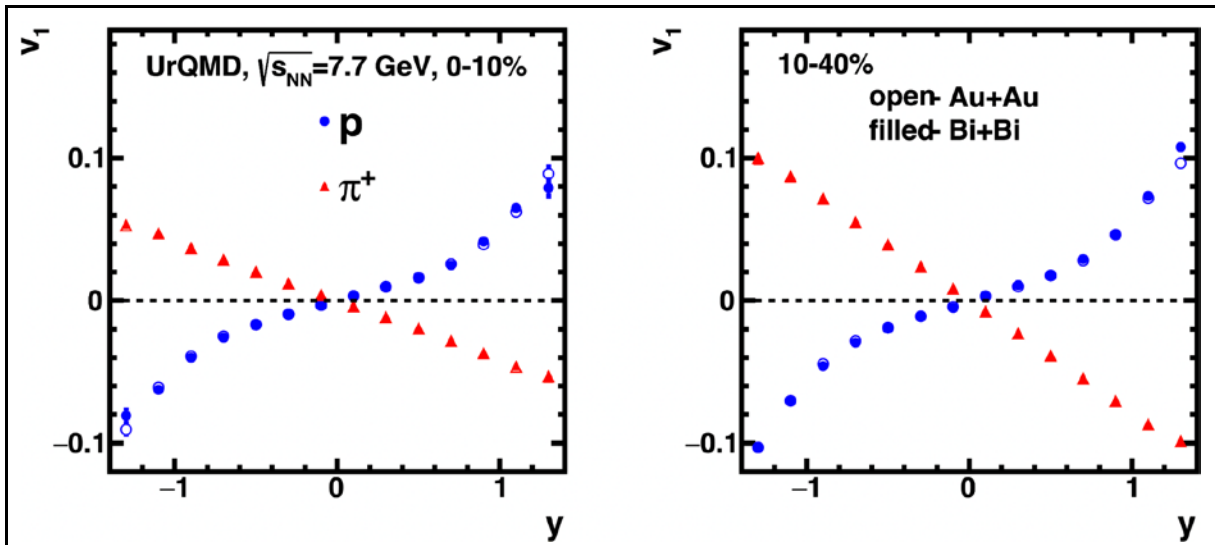


Figure 31. Rapidity y dependence of directed v_1 flow of charged pions and protons for 0–10% central (left panel) and 10–40% central (right panel) collisions at $\sqrt{s_{NN}} = 7.7$ GeV. Open symbols represent results for Au + Au and closed symbols for Bi + Bi collisions.



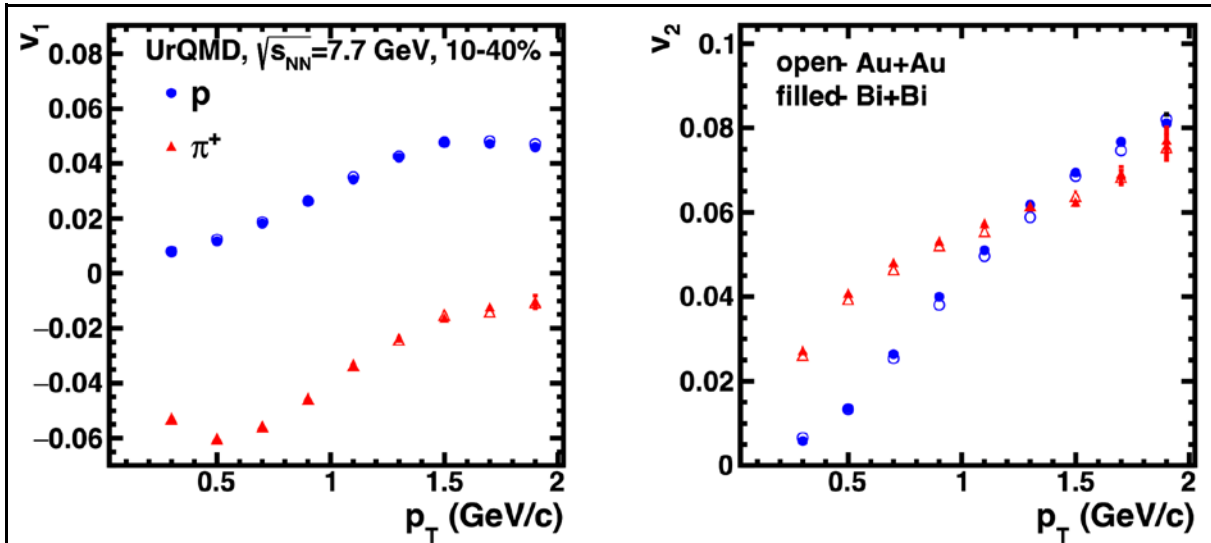


Figure 32. p_T dependence of directed v_1 flow (left panel) and elliptic flow v_2 (right panel) of charged pions and protons for 10–40% central heavy-ion collisions at $\sqrt{s_{NN}}=7.7$ GeV. Open symbols represent results for Au + Au and closed symbols for Bi + Bi collisions.

3.4 Summary

A procedure for centrality determination based on charged hadron multiplicity is established for the Multi-Purpose Detector (MPD) experiment at NICA. The connection between the averaged impact parameter and centrality classes was extracted using the multiplicity of the produced charged particles at midrapidity. The Monte-Carlo Glauber model and Γ -fit methods have been used to map the multiplicity of charged particles and impact parameter in a given centrality class. The validity of the procedure has been assessed using the generated and fully reconstructed transport model UrQMD data for Au + Au collisions at $\sqrt{s_{NN}}=4.5, 7.7,$ and 11.5 GeV. In the future, we plan to extend the MC-Glauber and Γ -fit fitting procedures for the energy of particles detected in the forward rapidity region by forward hadronic calorimeter FHCAL (MPD), which is sensitive to the spectator fragments.

The performance of the MPD experiment for directed (v_1) and elliptic (v_2) flow measurements was studied with Monte Carlo simulations using $^{198}\text{Au} + ^{198}\text{Au}$ and $^{209}\text{Bi} + ^{209}\text{Bi}$ collisions at NICA energies. A large sample of generated UrQMD minimum bias events has been used as an input for the full chain of realistic simulations of the MPD detector subsystems based on the GEANT4 platform and reconstruction algorithms built in the MPDROOT. Realistic procedures for centrality determination, particle identification and event plane reconstruction have been used in the analysis. The resulting performance of the MPD has been verified for v_1 and v_2 measurements of identified charged pions, kaons, protons, K^0_s and Λ particles as a function of rapidity and transverse momentum in different centrality classes. The detailed comparison of the results obtained from the analysis of the fully reconstructed data and generator-level data has allowed us to conclude that the MPD system will provide the detailed differential measurements of directed and elliptic flows with high efficiency. In future we plan to include the multiparticle methods of flow measurements, the data from other transport models and extend the study to other colliding systems.

References

- [1] P. Senger, *Particles* 4 (2021) 2, 214-226



- [2] M. Baznat et al., Phys. Part. Nucl. Lett. 17 (2020) 3, 303-324 // DCM-QGSM
- [3] S. Agostinelli et al., Nucl. Instrum. Meth. A 506 (2003) 250-303 // Geant4
- [4] The CBM collaboration: Technical Design Report for the CBM Time-of-Flight System (TOF) (2014)
- [5] The ALICE Collaboration, Eur.Phys.J.Plus 131 (2016) 5, 168
- [6] I. Kisel et al., JPCS 1602, 012006 (2020)
- [7] M. Miller et al., Ann.Rev.Nucl.Part.Sci. 57 (2007), 205-243
- [8] S.A. Bass et al., Prog. Part. Nucl. Phys. 41 (1998) 255–369 // Urqmd
- [9] V. Klochkov, I. Selyuzhenkov JPCS 798(1):012059
- [10] S. Voloshin et al. Landolt-Bornstein 23 (2010) 293-333
- [11] I. Selyuzhenkov Phys. Rev.C 77 (2008) 034904
- [12] <https://git.cbm.gsi.de/pwg-c2f/analysis/centrality>
- [13] A. Taranenko, J. Phys.: Conf. Ser. 1685 (2020) 012021
- [14] A. Zinchenko et al., J. Phys. Conf. Ser. 1390 (2019) 012017
- [15] S. Tarafdar et al., Nucl. Instrum. Meth. A 768 (2014) 170–178
- [16] R. Roglyet al., Phys. Rev. C 98 (2018) 024902 [CrossRef]
- [17] S.J. Das et al., Phys. Rev. C 97 (2018) 014905 [CrossRef]
- [18] L. Adamczyk et al., Phys. Rev. C 88 (2013) 014902
- [19] C. Loizides et al., SoftwareX 1–2 (2015) 13–18 [CrossRef]

4. Summary and outlook

The development of common software packages for simulation and data analysis for MPD experiments at NICA and the CBM experiment at FAIR has commenced. The common frameworks for centrality determination and anisotropic flow measurements are developed and tested. The MPD and CBM performance for the flow measurement of protons and charged pions and kaons has been investigated with the available heavy-ion event generators. The detailed comparison of the results obtained from the analysis of the fully reconstructed data and generator-level data has allowed us to conclude that the MPD and CBM systems will provide the detailed differential measurements of directed and elliptic flows with high efficiency.

Results of the project have been presented in 21 presentations at the major international physics conferences and workshops in 2020-2021 and the CBM, MPD and BM@N Collaboration meetings with acknowledgements to the CREMLINplus funding. A series of international workshops aimed to promote scientific exchange and development of novel ideas in the area of common software packages for simulation, data analysis, and studies determining physics performance at future FAIR and NICA experiments has been started at MEPHl and three workshops in 2020-2021 were organized with the next workshop planned for March 2022. In future, the studies of flow harmonics will be performed for strange hyperons and extended for the BM@N experimental setup. The activities within Task 2.7 are according to schedule.

5. Publications 2020-2021

- [1] A. Taranenko, J. Phys.: Conf. Ser. 1685 (2020) 012021 [CrossRef]
- [2] D. Idrisov, P. Parfenov et al., J. Phys.: Conf. Ser. 1690 (2020) 012129 [CrossRef]
- [3] I. Segal, O. Golosov et al., J. Phys.: Conf. Ser. 1690 (2020) 012107 [CrossRef]
- [4] I. Selyuzhenkov J. Phys.: Conf. Ser. 1685 (2020) 012020 [CrossRef]
- [5] O. Golosov, E. Kashirin et al., Particles 4 (2021), 3 354-360 [CrossRef]
- [6] O. Lubynets, I. Selyuzhenkov et al., Particles 4 (2021), 2 288-295 [CrossRef]



- [7] M. Mamaev, O. Golosov et al., J. Phys: Conf. Ser. 1690 (2020), 1 012122 [[CrossRef](#)]
- [8] D. Idrisov, P. Parfenov et al., Physics of Particles and Nuclei 52 (2021), 4 637-643 [[CrossRef](#)]
- [9] P. Parfenov et al., Physics of Particles and Nuclei 52 (2021), 4 618-623 [[CrossRef](#)]
- [10] P. Parfenov et al., Particles 4 (2021), 2 275-287 [[CrossRef](#)]
- [11] A. Taranenko et al., Acta Phys. Polonica B Proceedings Supplement 14 (2021), 3 515 [[CrossRef](#)]
- [12] P. Parfenov et al., Acta Phys. Polonica B Proceedings Supplement 14 (2021), 3 503 [[CrossRef](#)]
- [13] V.B. Luong, P. Parfenov et al., AIP Conference Proceedings 2377 (2021) 030011 [[CrossRef](#)]
- [14] A. Demanov, A. Taranenko et al., AIP Conference Proceedings 2377 (2021) 030003 [[CrossRef](#)]

